Bioorganic Chemistry 153 (2024) 107817

Contents lists available at ScienceDirect

Bioorganic Chemistry

journal homepage: www.elsevier.com/locate/bioorg

Tetrahydrocarbazoles incorporating 5-arylidene-4-thiazolinones as potential antileukemia and antilymphoma targeting tyrosine kinase and tubulin polymerase enzymes: Design, synthesis, structural, biological and molecular docking studies

Basma S. Ali [a], Anber F. Mohammed [a], Benson M. Kariuki [b], Raafat El-Awady [c], Hajjaj H. M. Abdu-Allah [a,*]

[a] Pharmaceutical Organic Chemistry Department, Faculty of Pharmacy, Assiut University, Assiut 71526, Egypt
[b] School of chemistry, Cardiff university, Cardiff CF10 3AT UK
[c] Research Institute for Medical and Health Sciences and College of Pharmacy, University of sharjah, Sharjah 27272, United Arab Emirates

ARTICLE INFO

Keywords:
Tetrahydrocarbazole
4-thiazolinone
Delépine reaction
Leukemia
Lymphoma
Tyrosine kinase
Tubulin

ABSTRACT

Finding effective and selective anticancer agents is a top medical priority due to high clinical treatment demand. However, current anticancer agents have serious side effects and resistance development remains a big concern. This creates an urgent need for new multitarget drugs that could solve these problems. Tetrahydrocarbazoles and 5-arylidene-4-thiazolinones have always attracted researchers for their multifaced anticancer activities and the possibility to be easily derivatized. Thereby, herein we report the combination of the two scaffolds to provide compounds **9a-j** and **10a-j** that were fully characterized and their tautomeric form was confirmed by crystal structure. **9a-j** and **10a-j** were assessed for *in vitro* antiproliferative activity using SRB assay against a panel of seven human cancer cell lines with doxorubicin as the standard. The results revealed that the cell lines derived from leukemia (Jurkat) and lymphoma (U937) are the most sensitive. Compounds **9d**, **10e**, **10g**, and **10f** revealed the highest potency (IC_{50} = 3.11–11.89 μM) with much lower effects on normal lymphocytes cell line (IC_{50} > 50 μM). The results show that modifications at 6th position of the THC and the nature of the substituent at the arylidene moiety affect the activity. To exploit the mode of action, **9d**, **10e, 10f**, and **10g** were evaluated as VEGFR-2 and EGFR inhibitors. **10e** is the most potent (IC_{50} 0.26 and 0.14 μM) against both enzymes. It also induced G0-G1-phase cell cycle arrest and apoptosis. While **10g** exhibited higher potency (IC_{50} 9.95 μM) than vincristine (IC_{50} 15.63 μM) against tubulin. A molecular docking study was carried out to understand the interactions between **10e**, **10g** and their targets. This study reveals **10e** and **10g** as possible candidates for developing multitarget anticancer agents against leukemia and lymphoma.

1. Introduction

Despite intensive ongoing research, cancer remains one of the most prevalent and aggressive diseases worldwide. In 2022, cancer was estimated to be the cause of 9.7 million deaths worldwide, of which 0.7 are due to blood cancer [1]. Blood cancers impact on the formation and activity of blood cells. Leukaemia, lymphoma and myeloma are amongst the most common types of blood cancer [2]. The main obstacles to the current chemotherapy of cancer include acquired resistance, undesirable side effects, high cost, and lack of selectivity often due to drug combination [3,4]. Multiple drugs are frequently used in virtue of the multifactorial and multi-mechanistic nature of cancer. An approach to the challenge is to focus on the development of multitargeting drugs which could be more effective in decreasing multidrug resistance, side effects, reducing treatment cost, and increasing response rates [5]. Protein tyrosine kinases (PTK) are regarded as crucial targets in cancer therapy because they are overexpressed/mutant in different types of cancers. Moreover, their signaling triggers a molecular cascade that can result in cell expansion, multiplication, migration, and angiogenesis [6]. Thus, development of PTK inhibitors is an established strategy for fighting cancer [7]. Vascular endothelial growth factor (VEGFR) and epidermal growth factor (EGFR) are examples of PTK. They are closely

* Corresponding author.
E-mail address: hajjaj@aun.edu.eg (H. H. M. Abdu-Allah).

https://doi.org/10.1016/j.bioorg.2024.107817
Received 11 July 2024; Received in revised form 23 August 2024; Accepted 8 September 2024
Available online 10 September 2024

related, as EGFR expression causes an upregulation of VEGFR signaling and both play a role in the development of several tumor types [8,9]. As a result, they are an attractive target for the development of new anticancer drugs [10]. VEGFR is an essential mediator in the regulation of cancer angiogenesis, endothelial cell migration, propagation, and other biological processes. There are three subtypes, namely, VEGFR-1, VEGFR-2, and VEGFR-3. VEGFR-2 is the most essential factor for angiogenesis as it is much distributed throughout vascular endothelial cells and serves as a key angiogenesis signal transducer and is associated with a much stronger kinase activity than VEGFR-1 and VEGFR-3 [11,12]. EGFR is overexpressed in various types of leukemic, lymphatic, and multiple myeloma cell lines due to its role in cancer development; signal transduction, survival, multiplication, formation of metastases, cell cycle regulation and anti-apoptosis signaling [13–15].

Microtubules, the essential protein for controlling the polymerization of the mitotic spindles, maintenance of cell shape, proliferation, motility, angiogenesis, and apoptosis, are involved in the progression of lymphoma and leukemia [16,17]. Therefore, tubulin polymerase inhibition also, is a key target in the creation of blood cancer medications.

Our rationale leads to design multi-target inhibitors, in contrast to single-target inhibitors for concurrently attacking tubulin, VEGFR-2 and EGFR [18]. An effective method for creating a multitarget drug is by combining various privileged heterocyclic pharmacophores into one single molecule. The tetrahydrocarbazole (THC) pharmacophore is ubiquitous in natural products and biologically active compounds. It is a 2, 3-disubstituted indole derivatives and is an important scaffold in synthesizing anticancer agents [19–28]. THC is a relevant scaffold in natural products and synthetic anticancer drugs with widely varying modes of actions. Vincristine and vinblastine are just to name a few. Both are very effective in the treatment of leukemia and lymphoma through tubulin polymerase inhibition [19–21]. Interestingly, some of THC derivatives are clinically approved in blood cancer treatment, such as midostaurin and emvododstat (Fig. 1), through VEFGR-2 inhibition activity [22,23].

Additionally, a number of THC derivatives (Fig. 1) are reported to act as anticancer agents through diverse mechanistic pathways, such as protein kinase casein kinase 2 (CK2) inhibitors (e. g. compound **I**) [24], cyclooxygenase-2 (COX-2) inhibitors (e. g. compound **II**, $IC_{50} = 0.1$ μM) [25], G-protein coupled receptor ligands (e. g. compound **III**, $EC_{50} = 7$ nM) [26], histone deacetylase (HDAC) inhibitors (e. g. compound **IV**) [27], and interfering with the cell cycle, apoptosis, and cell division [19,28].

Another group of common scaffolds used in the development of novel anticancer agents in the modern medicinal chemistry are the 4-thiazolinones [29]. Derivatives of 4-thiazolinone (Fig. 2) have shown promising antiproliferative activities against various cancers cell lines including leukemia [30], melanoma, lung, colon, CNS, ovarian, renal, prostate, and breast cancers [31,32]. They (Fig. 2) function through mechanisms such as inhibition of EGFR (e. g. compound **V**, $IC_{50} = 0.23$ μM) [33], VEGFR-2 (e. g. compound **VI**, $IC_{50} = 0.38$ μM) [34], tubulin enzymes (e. g. compound **VII**, $IC_{50} = 2.9$ μM) [35], apoptosis induction (e. g. compound **VIII**) [36], and cell cycle arrest [37]. In the search for the best moiety for anticancer agents among the 4-thiazolinone derivatives, 5-arylidene-2-amino-4-thiazolinones were particularly promising [38].

The multiple anticancer mechanisms of both THC and 4-thiazolinone make them attractive pharmacophores for molecular hybrid design. Thus, the current study describes the synthesis of novel hybrids of both moieties to combine their biological pharmacophoric characteristics in a single framework with the aim of obtaining multitarget anticancer agents (Fig. 3). Selected arylidene substituents were introduced at the fifth position of 4-thiazolinone moiety [39–43] to explore their electronic and steric effects on antiproliferative activity. Moreover, previous studies revealed that the substitution at the sixth position of the THC moiety with lipophilic group like chloro enhances the anticancer activity [44–46]. The target hybrids were synthesized, characterized and evaluated for their antiproliferative activity against a panel of seven cancer

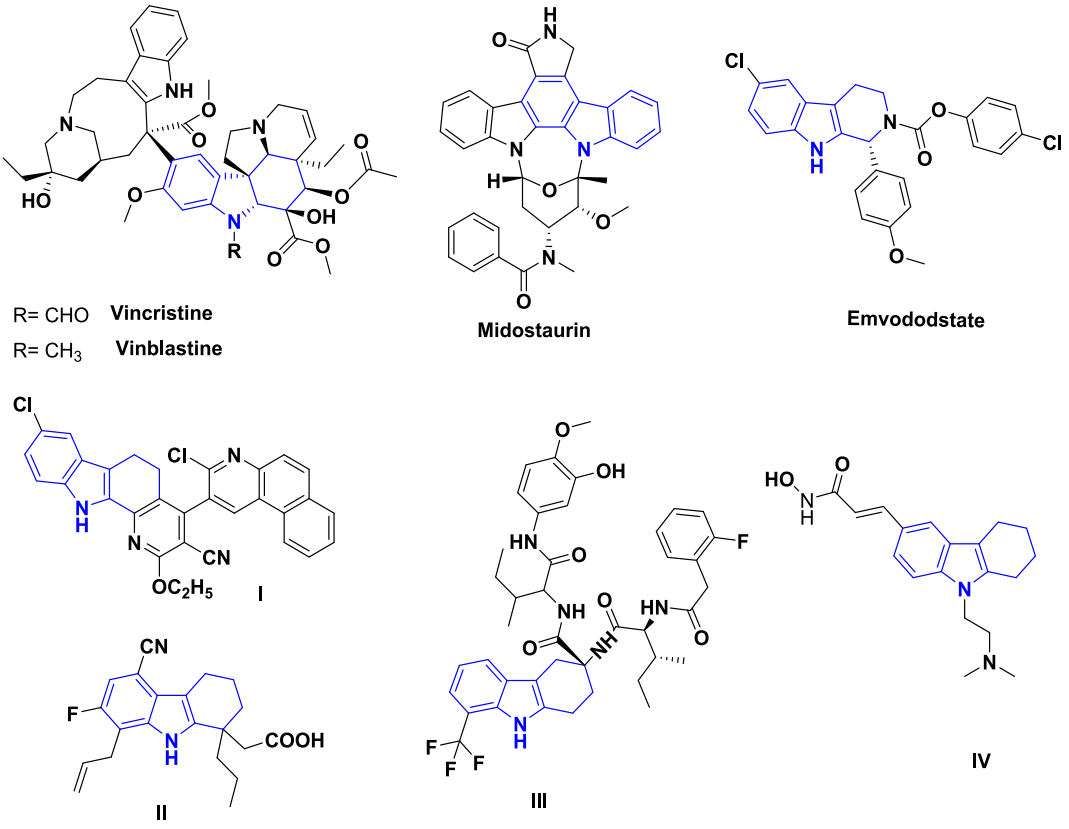

Fig. 1. Chemical structures of clinically used drugs and of a selection of anticancer agents with the THC scaffold.

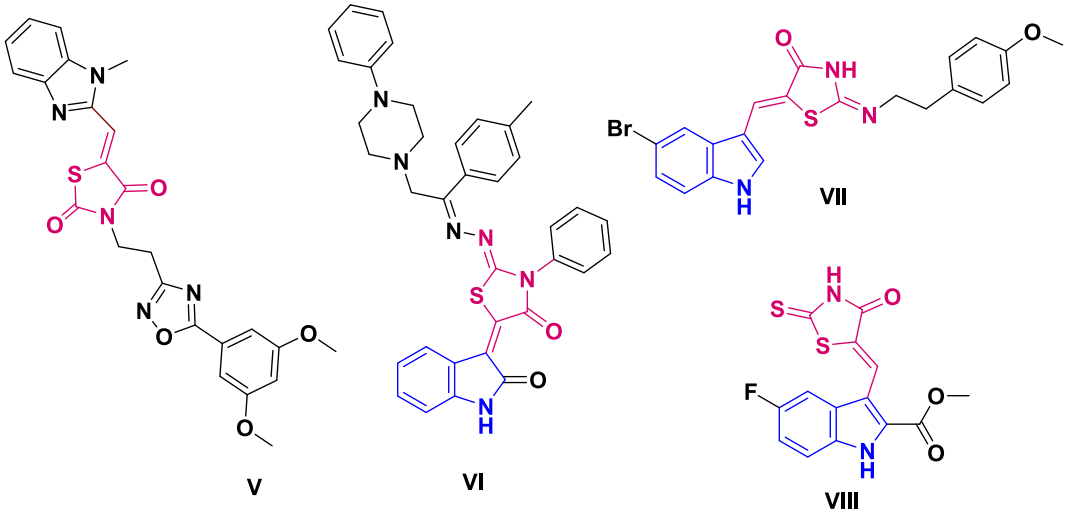

Fig. 2. Anticancer agents with 4-thiazolinone scaffold.

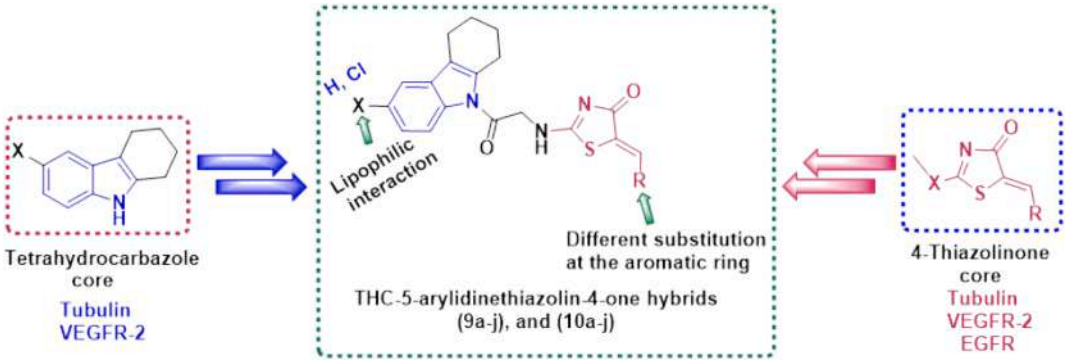

Fig. 3. Design of THC 4-thiazolinone hybrids (**9a-j)** and (**10a-j)** as potential multitarget anticancer agents.

cell lines compared with doxorubicin. The compounds with the best antiproliferative activities were subjected to mechanistic studies including cell cycle analysis, apoptosis assay, tubulin polymerase, EGFR and VEGFR-2 inhibitory activities.

2. Results and discussion

2.1. Chemistry

The synthesis of the designed target compounds; (**9a-j)** and (**10a-j**), was achieved following the pathways presented in Schemes 1 and 2.

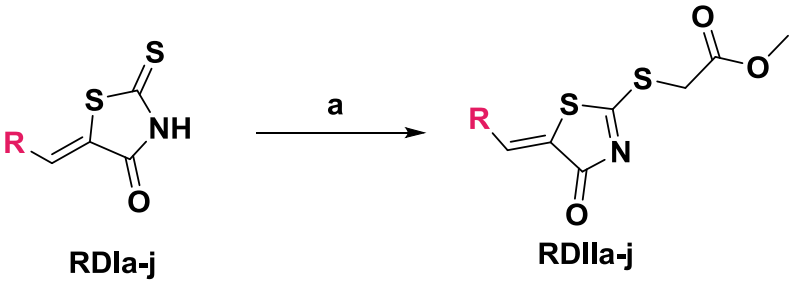

a; R = 4-ClC$_6$H$_4$
b; R = 4-BrC$_6$H$_4$
c; R = 4-MeC$_6$H$_4$
d; R = 4-(Me)$_2$NC$_6$H$_4$
e; R = 2-OH-C$_6$H$_4$
f; R = 4-OH-C$_6$H$_4$
g; R = 4-MeOC$_6$H$_4$
h; R = 3,4-(MeO)$_2$C$_6$H$_3$
i; R = 3,4,5-(MeO)$_3$C$_6$H$_2$
j; R = CH=CH-C$_6$H$_5$

Scheme 1. Synthesis of rhodanine derivatives RDIIa-j. Reagents and conditions: (a) Methyl bromoacetate (1.2 eq.), TEA (1 eq.), dry acetone, reflux, 4–7 h, 60–93 % yield.

Target hybrids comprise two main scaffolds; 5-arylidene-4-thiazolinone and THC. Rhodanine was used as the starting material for introducing 5-arylidene-4-thiazolinones through the synthesis of derivatives **RDIIa-j** (Scheme 1). Rhodanine itself was prepared from the reaction of chloroacetic acid with ammonium thiocyanate [47]. Knoevenagel condensation reaction between rhodanine and the selected benzaldehydes and cinnamaldehyde provided ten arylidenerhodanine derivatives (**RD**Ia-j) [48], Compounds (**RD**Ia-j) were S-alkylated with methyl bromoacetate in acetone in presence of triethylamine (TEA) to afford rhodanine derivatives **RD**IIa-j (Scheme 1). **RD**IIa-j are new compounds except for RD**IIa**, **RDIIc**, **RDIIf**, and **RDIIg** which have been reported but without NMR characterization [49]. Structures of **RD**IIa-j were verified by the appearance of C═O peak and disappearance of C═S (SH) stretching in IR spectra, while their ^{1}H NMR spectra showed two singlet signals corresponding to CH_2, and CH_3 of the methyl ester. **RD**IIa-j were used for introducing 5-arylidene-4-thiazolinone upon reaction with aminotetrahydrocarbazole derivatives **7** and **8** (Scheme 2). **7** and **8** were synthesized as follow: the starting tetrahydrocarbazoles (**3** and **4**) were obtained by Fischer indole synthesis reaction condition between phenylhydrazine HCl (**1**), or 4-chlorophenylhydrazine HCl (**2**) and cyclohexanone [50–53]. **2** was prepared by sodium sulfite reduction of diazonium salt of 4-chloroaniline [54]. Bromoacetylation of **3** and **4** were achieved via reaction with bromoacetyl bromide in $CHCl_3$ to obtain the bromoacetamide derivatives 5 and 6. Both are new compounds and were characterized by the appearance of the C═O peak at 1714 cm^{-1} in IR, and a singlet signal for CH_2 Br at 4.35 ppm in ^{1}H NMR. For the synthesis of the amino derivatives **7** and **8**, several trials were performed under different reaction conditions including Gabriel synthesis or heating with ammonia solution. However, vigorous conditions of these reactions, heating under basic conditions, hydrolyzed the amide bond of compound **5**. Alternatively, azidation of **5** followed by reduction with triphenylphosphine was also tried but purification of the amine was difficult even by column chromatography due to the presence triphenylphosphine oxide. Also, the reduction of azide by lithium aluminum hydride or sodium borohydride was tried, but it was impractical. The most appropriate method for amination of the active alkyl bromides **5** and **6** was found to be under Delépine reaction condition. Delépine reaction is useful for the conversion of alkyl halides to primary amines and has the advantages of cheap reagent, simple reaction condition and apparatus, and short reaction time [55]. The reaction proceeds via an S_N2 displacement of hexamethylenetetramine on substrates **5** and **6** in $CHCl_3$, followed by cleavage of the resulting salt with ethanolic HCl to afford compounds **7** and **8 in** high yield (82 %) and purity. Their structures were confirmed by the appearance of a broad band in the IR spectra at 2500–3369 cm^{-1} corresponding to NH_2HCl.

Finally, THC and 5-arylidene-4-thiazolinone hybrids (**9a-j**) and (**10a-j**) were synthesized under condition reported for similar compounds [56]. Therefore, treatment of the primary amine **7** or **8** with the appropriate rhodanine derivative **RDIIa-j** in ethanol and in presence of TEA afforded the target compounds (**9a-j**) and (**10a-j**). The reaction occurs through nucleophilic substitution mechanism. The structures of all target hybrids were confirmed by spectroscopic (IR, ^{1}H, and ^{13}C NMR) and elemental analyses. The ^{1}H NMR spectra indicated the appearance of signals characteristic of both 4-thiazolinone and THC moieties. The $\underline{NH}CH_2$ proton appeared as a broad singlet in some compounds such as (**9b**) or as triplet such as (**9c**) in the range of 9.98–10.27 with *J* coupling constant 5.1–5.7 Hz. Additionally, ^{13}C NMR spectra of the synthesized compounds revealed the presence of two C═O carbons at 178.9–180.0 and 173.9–175.3 ppm, aliphatic carbons of THC at 49.9–20.6 ppm.

Due to possible prototropic tautomerism of 2-amino-4-thiazolinones, it can primarily exist in two tautomeric forms: amino and imino form. Depending on the nature of the substituent at the 2-position. In case of *N*-phenyl or *N*-alkyl, the amino form is predominant [39–43,57], while *N*-heterocycles exist in imine form [58]. However, compound **VII,** with aliphatic linker, is reported in the imino form [35].

Thus, to explore the tautomeric form of the target compounds (**9a-j**) and (**10a-j**), X-ray crystallography was measured for some compounds. The X-ray single crystal analysis (Fig. 4) of **9b** and **9j**, along with NMR, revealed that the form with the exocyclic amine NH is the predominant one.

The crystal structure of **9b** is triclinic, and its asymmetric unit consists of one molecule of **9b** and a molecule of DMSO solvent (Fig. S1 (a)). In the structure, N—H…O hydrogen bonding occurs between the amide group and the oxygen atom of the DMSO solvent as shown in Table S2 and (Fig. S1 (b)). The crystal structure of **9j** is monoclinic. The

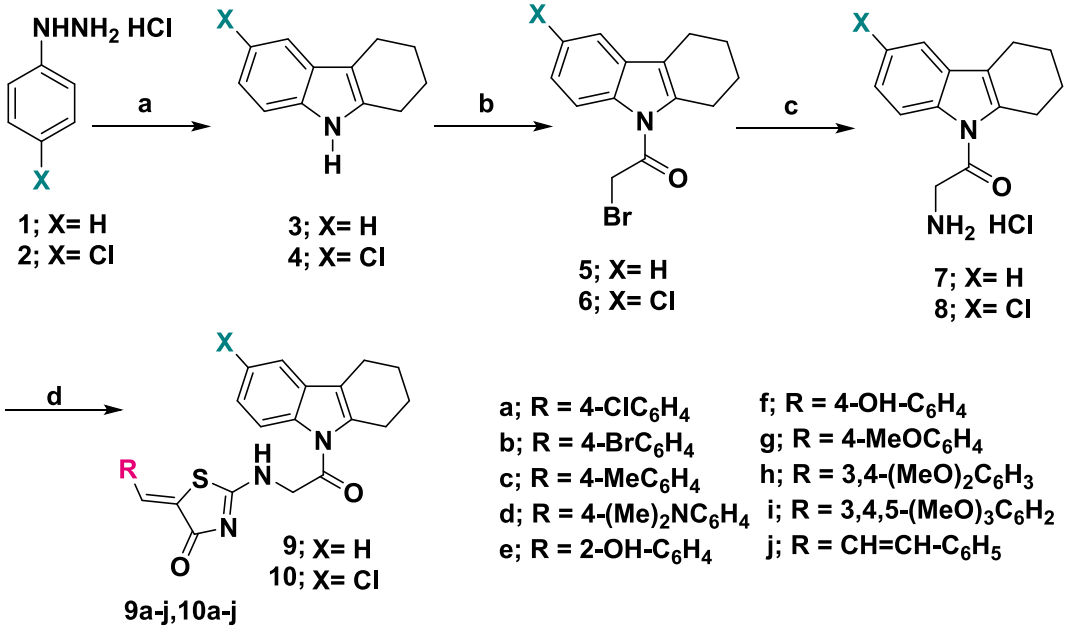

Scheme 2. Synthesis of tetrahydrocarbazole 5-arylidene-4-thiazolinone hybrids 9a-j and **10a-j.** Reagents and conditions:(a) cyclohexanone (1.2 eq.), sodium acetate (1.2 eq.), glacial acetic acid, reflux, 6 h, 76–80 % yield; (b) Bromoacetyl bromide (2 eq.), $CHCl_3$, reflux, 7 h, 73–74 % yield; (c) i) Hexamethylenetetramine (1.1 eq.), $CHCl_3$, reflux, 5 h, 83–84 % yield; ii) HCl, EtOH, 18 h, 81–82 % yield; (d) **RDIIa-j**, TEA, EtOH, reflux, 7–10 h, 19–56 % yield.

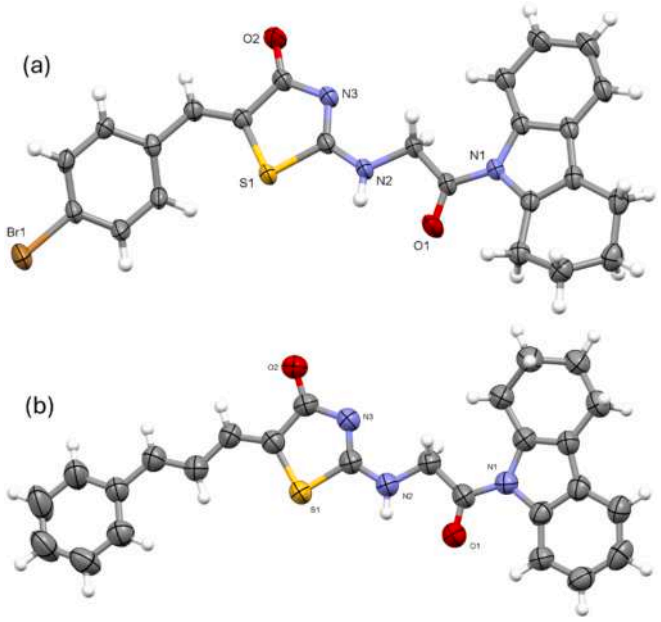

Fig. 4. Ortep represantations of molecules of (a) **9b** and (b) **9j** obtained by single crystal structure determination.

asymmetric unit consists of two independent molecules of **9j** and two molecules of ethanol solvent (Fig. S2 (a)). The crystal structure shows that the partially saturated cyclohexane ring exists in half chair conformation. In the crystal, the amide groups of both independent molecules form N—H…O hydrogen bonds with the oxygen atoms of an ethanol molecule (Table S2, Fig. S2 (b)). The ethanol molecule forms a O—H…O bond to the second independent solvent molecule which in turn bonds with the oxygen atom of the 4-thiazolinone group.

2.2. Biology

2.2.1. Anti-proliferative activity

All the target hybrids **9a-j** and **10a-j** were initially evaluated for their *in-vitro* antiproliferative activity using sulforhodamine B (SRB) assay at 10 μM concentration against a panel of representative seven human cancer cell lines: hormonal positive breast cancer (MCF7), triple negative breast cancer (MDA-MB-231), colon cancer (HCT116), lung cancer (A549), glioblastoma (U87), leukemia (Jurkat), and lymphoma (U937), using doxorubicin as a positive control. The preliminary results of initial screening reveal that most of the tested compounds showed high antiproliferative activity against three cell lines [colon cancer (HCT116), leukemia (Jurkat) and lymphoma (U937)] (Fig. S3-S9). Also, the results display that 6-chloroTHC derivatives **10a-j** have better antiproliferative activity than non-chlorinated derivatives **9a-j,** particularly, against U937 and HCT116 cell lines. Moreover, the number of methoxy groups has a significant impact on the anti-proliferative activity. preliminary study revealed that increasing number of methoxy groups results in dramatic decrease in activity (Fig. S4, S6, and S7). Compounds **9c**, **9d**, **10a**, **10c**, **10e**, **10f**, **10g**, and **10h** showed the highest inhibitory activity against Jurkat (Fig. S6), while **10e, 10f**, **10g**, and **10h** were the most active against HCT116 (Fig. S4). Furthermore, the most active anti-proliferative compounds against the lymphoma U937 were **10a**, **10c**, **10e**, **10f**, **10g**, and **10h** (Fig. S7). To determine IC_{50} of the most active compounds, they were tested at different concentrations (0,01 – 50 μM). The relationship between cell viability and drug concentration was plotted to obtain a full concentration–response survival curve. Three separate experiments in triplicate were done to assess the potential IC_{50} of each target compound (Fig. S10-S12). Results in Table 1 demonstrate that the modification of the arylidene moiety by adding different substituents produced notable differences in the compound's effectiveness

Table 1
IC_{50} values of **9c**, **9d**, **10a**, **10c**, **10e**, **10f**, **10g**, **10h** and doxorubicin (DOX) in cancer cell lines.

Compd. No.	X	R	IC_{50} (μM)[a] Jurkat	HCT-116	U937
9c	H	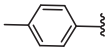	13.45 ± 0.08	NA[b]	NA[b]
9d	H	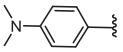	3.11 ± 0.11	NA[b]	NA[b]
10a	Cl	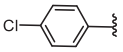	12.02 ± 0.09	NA[b]	14.00 ± 0.07
10c	Cl	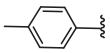	13.02 ± 0.07	NA[b]	NA[b]
10e	Cl		4.53 ± 0.08	11.94 ± 0.08	6.79 ± 0.09
10f	Cl	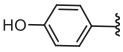	11.89 ± 0.09	11.64 ± 0.08	6.53 ± 0.09
10g	Cl	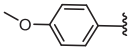	5.13 ± 0.09	35.12 ± 0.07	7.31 ± 0.08
10h	Cl	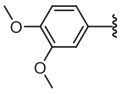	11.80 ± 0.08	34.36 ± 0.06	16.71 ± 0.09
DOX	–	–	0.09 ± 0.12	0.10 ± 0.12	0.05 ± 0.12

IC_{50} [a] values are the mean ± S.D. of three independent experiments. NA[b]: Not assayed compounds.

against colon cancer (HCT116), leukemia (Jurkat) and lymphoma (U937) cell lines. As explained above, substituents on benzylidene ring were selected based on previous studies [39–43]. Compounds with halogen atom (R=chloro or bromo) on the benzylidene ring showed a decrease in activity in comparison with donating group (R=methyl, dimethylamino, hydroxy or methoxy) (Fig. 10). Regarding activity against Jurkat cell line, compound **9d** (R=4-$(Me)_2NC_4H_6$) was the most potent with an IC_{50} of 3.11 μM, while compound **10e** (R=2-OH-C_4H_6) ranked the second with an IC_{50} of 4.35 μM. Moreover, compounds **10g** (R=4-$MeOC_4H_6$) and **10f** (R=4-OH-C_4H_6) revealed good activity with IC_{50} of 5.13, 11.89 μM, respectively. Turning to lymphoma (U937) and colon cancer (HCT116) cell lines, compound **10f** (R=4-OH-C_4H_6**)** was the most potent with IC_{50} of 6.53, 11.64 μM, respectively. Compound **10e** (R=2-OH-C_4H_6) also ranked the second with IC_{50} of 6.76, 11.94 μM. Although compound **10g** (R=4-$MeOC_4H_6$**)** ranked the third against lymphoma with an IC_{50} of 7.31 μM, it was the least potent derivative with IC_{50} of 35.12 μM against colon cancer cell line. Based on these findings, the most active compounds **9d**, **10e, 10f,** and **10g** were chosen for VEGFR-2, EGFR, tubulin polymerase inhibition assay.

2.2.2. Effect on normal lymphocytes

One requirement for a good anticancer agent is to show high activity against cancer cells with minimal or no activity on normal cells. To test the selectivity of our compounds, the anti-proliferative activity of the highly effective four derivatives **9d**, **10e**, **10f,** and **10g** was evaluated against normal human lymphocytes (PCS-800–017) using erlotinib as a reference drug. Table 2 shows that all compounds possess low cytotoxicity against normal cells with IC_{50} ranging from 87.84 to 242.09 μM in comparison with erlotinib with IC_{50} of 71.34 μM.

2.2.3. VEGFR-2 inhibition

VEGFR-2 has been reported to be overexpressed in blood cancers [59]. Thus, development of VEGFR inhibitors is a good strategy for

Table 2
IC_{50} values of **9d**, **10e**, **10f**, and **10g** compared to erlotinib in normal lymphocyte cells PCS-800–017.

Compd. No.	PCS-800–017 IC_{50} (μM)[a]
9d	161.44 ± 2.87
10e	131.67 ± 2.38
10f	242.09 ± 4.37
10g	87.84 ± 1.63
Erlotinib	71.34

IC_{50} [a] values are the mean ± S.D. of three experiments separately.

improvement of the treatment outcome of these cancers [60]. The four most potent compounds **9d**, **10e**, **10f,** and **10g** against Jurkat, and lymphoma cell lines were evaluated for their potential VEGFR-2 inhibition activity using sorafenib as a reference standard. The VEGFR-2 inhibitory assay revealed a promising inhibition activity of the tested compounds with IC_{50} 0.26–3.60 μM (Table 3). Among 6-chloroTHC derivatives **10e** (R=2-OH-C_4H_6) was the most potent with an IC_{50} value of 0.26 μM that is 1.5 fold less than that of sorafenib (IC_{50} value of 0.17 μM), while compound **10g** (R=4-MeOC_4H_6) ranked third with IC_{50} value of 1.05 μM, which is 3 fold more potent than compound **10f** (R=4-OH-C_4H_6) with IC_{50} value of 3.60 μM. Compound **9d** (R=4-$(Me)_2NC_4H_6$) among the THC derivatives ranked on the second position of the four tested compounds with IC_{50} value of 0.74 μM after compound **10e**.

2.2.4. EGFR inhibition

A correlation between EGFR and VEGFR has been previously reported. Human tumor cell lines that have activated EGFR have been shown to produce more angiogenic factors, including VEGFR, and EGFR blockade can lower the production of multiple angiogenic growth factors such as VGEFR [9]. Based on that the four tested compounds which were tested for VEGFR-2 inhibition assay were further evaluated for their potential inhibition activity against EGFR enzyme using erlotinib as a reference drug. Table 3 represents the EGFR inhibitory results, which reflects the promising inhibition activity of the tested compounds with IC_{50} ranging from 0.14 μM to 2.47 μM. Among 6-ChloroTHC derivatives **10e** (R=2-OH-C_4H_6) was the most potent with an IC_{50} value of 0.14 μM that was equipotent to erlotinib IC_{50} value of 0.11 μM, while compound **10g** (R=4-MeOC_4H_6) ranked second among the tested compounds with an IC_{50} value of 0.31 μM, which is 3 fold less potent than erlotinib. Compound **10f** (R=4-OH-C_4H_6**)** was the least potent compound among the tested derivatives with an IC_{50} value of 2.47 μM. Compound **9d** (R=4-$(Me)_2NC_4H_6$) ranked in the third position with an IC_{50} value of 0.87 μM.

Based on these results, compound **10e** (R=2-OH-C_4H_6) demonstrates excellent dual VEGFR-2/EGFR inhibition activity with the most potent IC_{50} of 0.26, 0.14 μM against both VEGFR-2 and EGFR, respectively.

Table 3
IC_{50} values of **9d**, **10e**, **10f**, and **10g** compared with erlotinib in EGFR inhibition assay, and sorafenib in VEGFR-2 inhibition assay.

Compd. No	IC_{50} (μM)[a] VEGFR-2	EGFR
9d	0.74 ± 0.01	0.87 ± 0.02
10e	0.26 ± 0.00	0.14 ± 0.00
10f	3.60 ± 0.06	2.47 ± 0.04
10g	1.05 ± 0.02	0.31 ± 0.01
Sorafenib	0.17 ± 0.00	NA[b]
Erlotinib	NA[b]	0.11 ± 0.00

IC_{50} [a] values are the mean ± S.D. of three independent experiments.
NA[b]: Not assayed compounds.

2.2.5. Tubulin inhibition

Since THC is structurally related to vinca alkaloids, which exert their anticancer effects mainly via inhibiting tubulin polymerization [20], and based on the kinase (VEGFR-2, and EGFR) inhibitory assay results, the three most potent compounds **9d**, **10e**, and **10g** were tested using tubulin polymerization assay with vincristine as a reference drug. Table 4 displays the tubulin inhibitory results. Compounds **9d**, **10e** and **10g** exhibits very good antimitotic activity with IC_{50} ranging from 9.95 μM to 40.90 μM. Regarding 6-chloroTHC derivatives, compounds **10e**, and **10g**, the most potent derivative was compound **10g** (R=4-MeO C_4H_6) with an IC_{50} value of 9.95 μM that was 1.5 more potent than vincristine (IC_{50} value of 15.63 μM), while compound **10e** (R=2-OH-C_4H_6) ranked third among tested compounds with IC_{50} value of 40.90 μM, which is 2.5 fold less potent than vincristine. Compound **9d** (R=4-$(Me)_2NC_4H_6$) with IC_{50} value equipotent to IC_{50} of vincristine, ranked in the second position among the chosen derivatives.

2.2.6. Cell cycle Analysis

The production of a novel drug that can control cell cycle progression and apoptosis is an appealing strategy for fighting cancer cells more precisely [61]. From the above data results, compounds **10e,** which showed dual excellent inhibition activity against both EGFR/VEGFR-2 compared to reference drugs was selected for cell cycle analysis in Jurkat using Propidium Iodide Flow Cytometry Kit. Fig. 5 shows the cell cycle histograms of the Jurkat cancer cells treated with compound **10e** and compared with those of the untreated cells. Compared to the control group, the percentage of compound **10e**-treated Jurkat cells in the G0-G1 phase (where the cell begins to grow before reproducing the DNA) was 1.3 times higher than the control. The percentage of the cell distribution increased from 46.28 % for the control to 61.67 % for **10e**-treated cells. This is in line with previous reports that showed that upon EGFR inhibition, tumor cells typically undergo apoptosis and cell cycle arrest at G0/G1 [62]. There was a decrease in the distribution of cells in both S and G2/M phases in comparison with the control.

2.2.7. Apoptosis assay

The induction of apoptosis was examined in Jurkat cells after treatment with compound **10e** and staining with annexin V/PI and compared with control (untreated Jurkat cells). Fig. 6. shows that the total percent of the Jurkat cells showing manifestations of early, and late stages of apoptotic cell death increased in cells treated with compound **10e** compared to the control cells. Compound **10e** presented a more significant level of apoptosis with a total percentage value of 35.44 in comparison with that of control one 2.71 %. This result validates the potential cell cycle inhibition and apoptotic activity of compound **10e**.

2.2.8. Molecular docking studies

In silico docking simulations were performed in order to investigate the binding modes of the most active anti-proliferative hybrids; **9d**, **10e**, **10f**, and **10g** at the target proteins. Molecular operating environment (MOE) platform [63] was utilized for ligand, protein preparation and docking simulations with Amber10:EHT forcefield and reaction field solvation model. X-ray crystal structure of VEGFR-2 in complex with Sorafenib was obtained from PDB with entry: 4ASD [64]. Self-docking

Table 4
IC_{50} values of **9d**, **10e**, and **10g** compared with vincristine in tubulin inhibition assay.

IC_{50} (μM)[a] Compd. No.	Tubulin
9d	15.40 ± 0.26
10e	40.90 ± 0.70
10g	9.95 ± 0.17
Vincristine	15.63 ± 0.47

IC_{50} [a] values are the mean ± S.D. of three independent experiments.

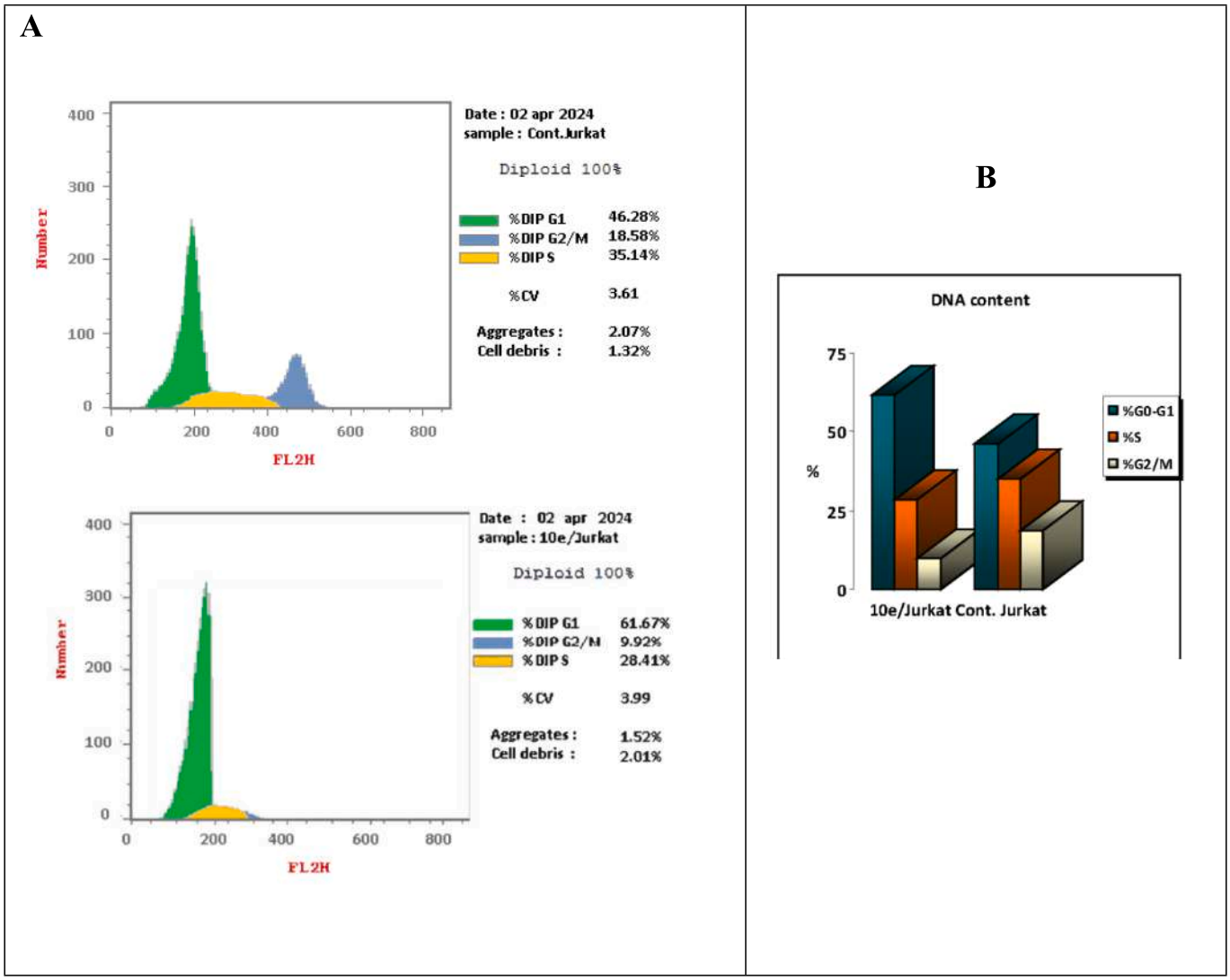

Fig. 5. Cell cycle analysis after treatment of the Jurkat cell with **10e**. A) analysis using flow cytometry to quantify the amount of DNA in control (upper) and **10e**-treated (lower) in Jurkat cell line. **B**) The histogram shows the distribution percentage of the cell cycle following **10e** treatment.

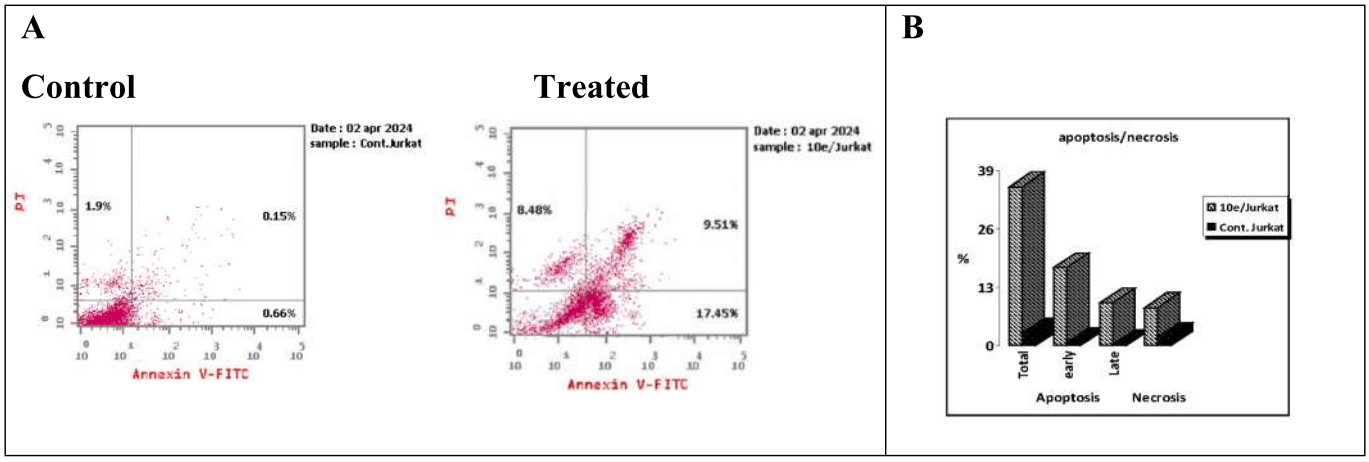

Fig. 6. Apoptosis induction analysis using compound **10e** in Jurkat cells after annexin V/PI staining. **A**) Flow cytometric display of a cell population exhibiting early/late apoptotic signs. **B**) percentage of cells exhibiting early, and late apoptosis, or necrosis presented quantitatively in relation to control cells.

was done before compounds' simulation to validate the docking protocol where the docked sorafenib displayed a *RMSD* value of 0.55 Å from the co-crystalized ligand (Fig. S16). Docked compounds result in good binding scores ranging from −7.77 to −8.70 kcal/mol compared with sorafenib (−10.06 kcal/mol). Simulation data of the compounds as well as sorafenib are shown in Table 5. Docking results revealed that the compounds bind snugly inside the elongated binding pocket. Comparable to 4-chloro-3-trifluorophenyl group of sorafenib (Fig. 7-C), the ligand THC scaffold fits tightly into the wide gate forming hydrophobic interactions with surrounding residues; Glu885, Asp1046, Leu1019, Ala866, Ile892, and Asp814. In addition to pi-H interactions with His1026 and Cys1045 are formed by THC moiety in **9d** and **10g** complexes. Also, the ligand methylene-amino linker donates two H bonds to Glu885 and Asp1046 by compounds (**10e** and **10f**), and a H bond to Asp1046 by **9d**. Regarding ligand 4-thiazolinone core, it forms *T*-stacking with Phe1046 and Cys1045 residues inside the pocket tunnel. Moreover, at the narrow hydrophobic gate, the ligand arylidene moiety stacks with Phe918 forming hydrophobic interactions with surrounding residues. Despite missing interaction with key Cys919 residue, the 2-hydroxybenzylidene moiety of **10e** aligns with the sorafenib pyridine ring and forms alternative H bond with adjacent Glu917 along with pi-H interaction with Val848 (Fig. 7-A and B**).** This interaction reinforces the binding complex of **10e** within the active site and might explain its higher potency relative to other congeners. Furthermore, the hybrids; **9d**, **10e**, **10f**, and **10g** were docked against the epidermal growth factor receptor tyrosine kinase EGFR to rationalize their potential dual kinase inhibition. The crystal structure of the EGFR in complex with erlotinib (PDB: 1 M17) [65] was used in the study. All minimizations were performed using the force field (OPLS-AA) as well as Born solvation model. Validation of the docking protocol was achieved by redocking the co-crystallized ligand into the EGFR binding site from where the docked ligand showed *RMSD* value of 1.48 Å (Fig. S17). Protein ligand poses exhibited good docking scores (−9.30 to −9.86 kcal/mol) relative to erlotinib docking score −10.70 kcal/mol. The simulation results of the compounds were compared with erlotinib and the data are shown in Table 6. Investigation of the ligand complexes revealed that the large binding pocket well tolerates the conformation of designed hybrids. The ligand arylidene moiety inserted into the hydrophobic pocket forming stacking with Phe699 along with hydrophobic interaction with Leu694, Val702, Phe771, Thr766, and Leu820. The Met742 residue accepts additional H bond from the dimethylamino group in **9d** complex**.** Also, Leu694 and Val702 residues form H-pi interactions with the ligand 4-thiazolinone spacer close to Met769 residue. Moreover, The Met769 amide nitrogen donates a H-bond to 4-thiazolinone core of **9d**, **10f** and **10g** compared to the H-bond with the quinazoline nitrogen of erlotinib (Fig. 8-C**).** However, rather than Met769, 2-hydroxybenzylidene group of **10e** donates unique H bond to Asp831 at the DFG motif, (Fig. 8-A and B**).** On the other side, the ligand THC scaffold occupies the gate of binding site forming stacking with Phe771 and Tyr777 as well as hydrophobic interactions with nearby residues; Asp776, pro770, Gly772, and Cys773. 6-Cl-THC moiety of **10e** projects past the erlotinib ether linkages forming additional pi-H interaction with Cys773, (Fig. 8-A and B**).** The results of docking simulations against VEGFR-2 and EGFR attributed to explain the antiproliferative effects of compounds **9d**, **10e**, **10f** and **10g** relative to their binding affinity within the active sites. Also, findings suggested that compound **10e** might act as a dual VEGFR-2 and EGFR kinase inhibitor.

Besides, the hybrids **9d, 10e**, and **10g** were docked at α/β-tubulin to investigate their potential binding mode and rationalize their multi-targeted effect. As a core pharmacophore in vincristine and vinblastine, indole as well as THC served significant contribution in interacting with vinca binding site. Therefore, initial docking study was done at the vinca binding site of tubulin using the crystal structure of tubulin-vinblastine complex (PDB: 5J2T) (Fig. S19)[66]. However, the docked compounds are relatively smaller than the cavity volume and lose specific interactions with nearby residues. Therefore, our study focused on the colchicine binding site of tubulin. Colchicine binding site (CBS) has a relatively small cavity volume and still attracts considerable interest as their targeting agents are much less prone to multidrug resistance (MDR) than are other microtubule destabilizing agents [67,68]. Docking simulations of the new hybrids were done using the crystal structure of combretastatin A4 (*cis*-CA-4) in complex with tubulin [PBD: 5LYJ][69]. CA-4 binds to the colchicine binding site and occupies the same space as microtubule-destabilizing agent colchicine (Fig. 9-C**).** The method was validated by redocking the co-crystallized ligand into the binding site where *RMSD* value obtained for the docked ligand was 0.45 Å (Fig. S20). Docked compounds exhibited stable complexes with docking scores ranging from −9.06 to −9.61 kcal/mol compared with CA-4 (−10.16 kcal/mol). The docking results of the compounds were compared with CA-4 and the data are represented in (Table 7). Analysis of the ligand complexes revealed that THC core of **9d** complex is deeply buried in a hydrophobic pocket shaped by residues βVal238, βCys241, βLeu242, βLeu248, βAla250, βLeu255, βAla316, βIle318, βAla354, and βIle378 forming pi-H interactions to βLeu255. The ligand 4-dimethylaminobenzylidene moiety is stacked between βAsn258 and βLys352 forming hydrophobic interactions to residues αThr179, αMet259, αAla316, and αAsn349. In addition, the 2-amino-4-thiazolinone moiety accepts a H bond from βAsp251. On the other hand, THC moiety of **10e** and **10g** is lying in a location that allows a stacking interaction between βAsn258 and βLys352 and the ligand is being upturned to donate halogen bond to βAsn349 rather than αThr179. Besides, the THC scaffold is stabilized by forming hydrophobic interactions to residues αThr179, αAla180, αVal181 αMet259, αAla316, and αAsn349. Moreover, the **10g** complex is further stabilized by donating H bond to βLys352 from 2-amino-4-thiazolinone moiety Fig. 9-A and B. The chloro-THC analogues; **10e** and **10g**, showed almost similar binding modes, although the 4-methoxy substituent is better tolerated within the hydrophobic pocket and its phenyl ring stacks between βCys241 and βLeu255 (Fig. 9-A**).** Moreover, alignment of **10g** complex onto *cis*-CA-4 one revealed that the 3-hydroxy-4-merhoxysubstituted ring of *cis*-CA-4 superimposes on the chloro-indole moiety of **10g**. However, THC moiety of **10g** is better tolerated within the hydrophobic pocket. Also, 4-methoxybenzylidene moiety of **10g** is buried deeper inside the pocket than is the 3,4,5-

Table 5
Ligand-protein complex interactions of the tested compounds **9d**, **10e**, **10f**, and **10g** within the binding site of VEGFR-2.

ompd.	MOE Score kcal/mol	H-bond interactions (Å)	Hydrophobic Interactions	Pi-H interactions (Å)
Sorafenib	−10.06	Cys919 (2.76, 3.55), Glu885 (3.04)	Val916, Leu889, Leu840, Asp1046, Cys1045 and Phe1047	Phe1047 (3.72)
9d	−8.70	Asp1046 (2.76)	Phe1047, Leu889, Leu840, Asp1046, and Cys1045	His1026 (4.24) Cys1045 (4.08)
10e	−7.89	Glu885 (3.02), Asp1046 (3.20) Glu917 (3.26)	Val916, Leu889, Leu840, Asp1046, Cys1045 and Phe1047	Val848 (4.70)
10f	−7.77	Glu885 (3.14), Asp1046 (2.91)	Leu889, Val916, Leu840, Asp1046, Cys1045 and	.....
10g	−7.98	.....	Cys1045, Val916, Leu889, Leu840, Asp1046, Cys1045 and Phe1047	Cys1045 (4.09)

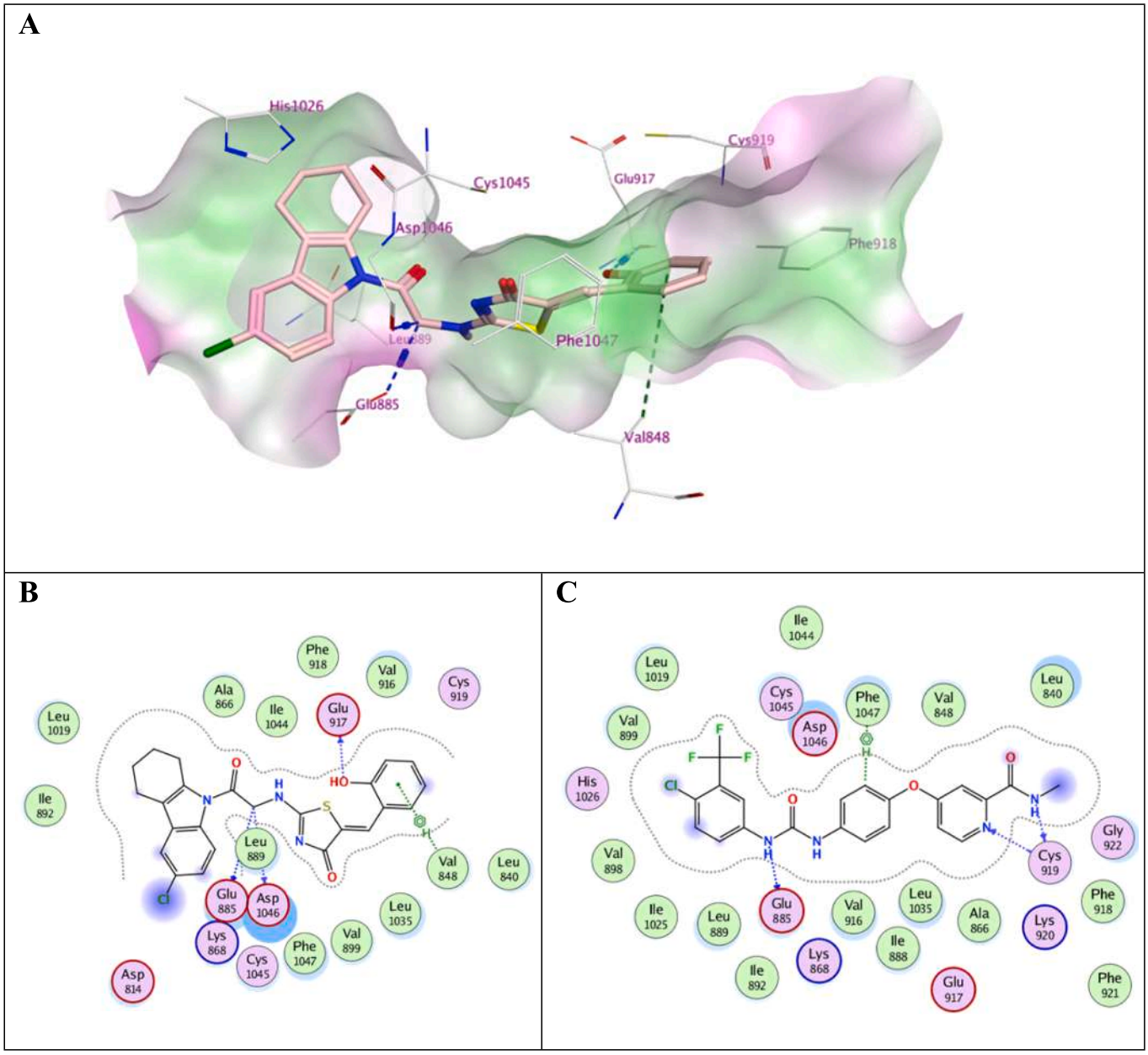

Fig. 7. Ligplots at VEGFR-2 binding site; A: 3D-docked model of compound **10e** (pink) showing the lipophilicity protein surface; (purple: hydrophilic, white: neutral, green: lipophilic) B: 2D-docked model of compound **10e**, C: 2D-docked model of sorafenib. (For interpretation of the references to color in this figure legend, the reader is referred to the web version of this article.)

Table 6
Ligand-protein complex interactions of the tested compounds **9d**, **10e**, **10f**, and **10g** within the binding site of EGFR.

Compd.	MOE Score kcal/mol	H-bond interactions (Å)	Hydrophobic interactions	Pi-H interactions (Å)
Erlotinib	−10.70	Met769 (3.68)	Leu694, Leu820, Val702, Gly722, Thr766, Thr830	Leu694 (4.27)
9d	−9.49	Met769 (2.95) Met742 (3.89)	Leu694, Leu820, Val702, Gly722, Thr766, Pro770	Leu694 (4.28) Val702 (4.95)
10e	−9.81	Asp831 (3.23)	Leu694, Leu820, Val702, Gly722, Thr766, Pro770, Glu780	Val702 (4.69) Cys773 (4.23)
10f	−9.86	Met769 (3.34)	Leu694, Leu820, Val702, Gly722, Thr766, Pro770, Glu780	–———————————
10g	−9.30	Met769 (2.97)	Leu694, Leu820, Val702, Gly722, Thr766, Pro770, Glu780, His781	Leu694 (4.05) Val702 (4.86)

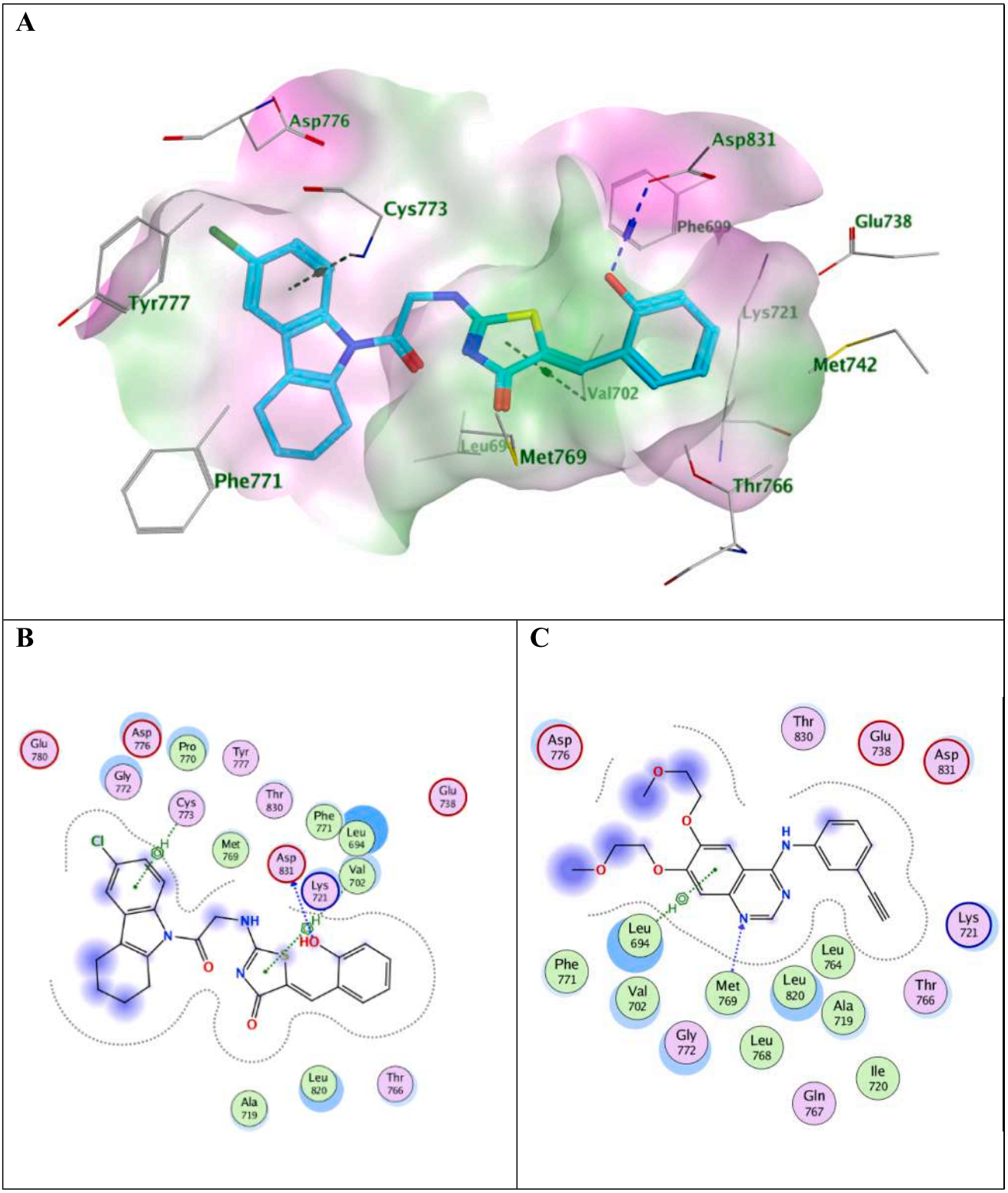

Fig. 8. Ligplots at EGFR binding site; A: 3D-docked model of compound **10e** (cyan) showing the lipophilicity protein surface; (purple: hydrophilic, white: neutral, green: lipophilic) B: 2D-docked model of compound **10e**, C: 2D-docked model of erlotinib. (For interpretation of the references to color in this figure legend, the reader is referred to the web version of this article.)

trimethoxysubstituted ring of *cis*-CA-4, (Fig. S21). Furthermore, induced fit docking was performed to further validate the data obtained from rigid receptor site. The simulation study confirmed the orientation acquired by chloro-THC derivatives; **10e** and **10g** as well as the upturned conformation of **9d** within the binding pocket. In addition, the complex of **10g** was further stabilized by a H bond interaction between 4-MeO substituent and Asn167 with 2.76 Å (Fig. S22). Docking simulations predict the binding modes of the most potent anti-proliferative hybrids at α/β-tubulin. Findings proposed the colchicine site as the plausible binging site for the most active hybrids; **9d**, **10e** and **10g** at α/β-tubulin

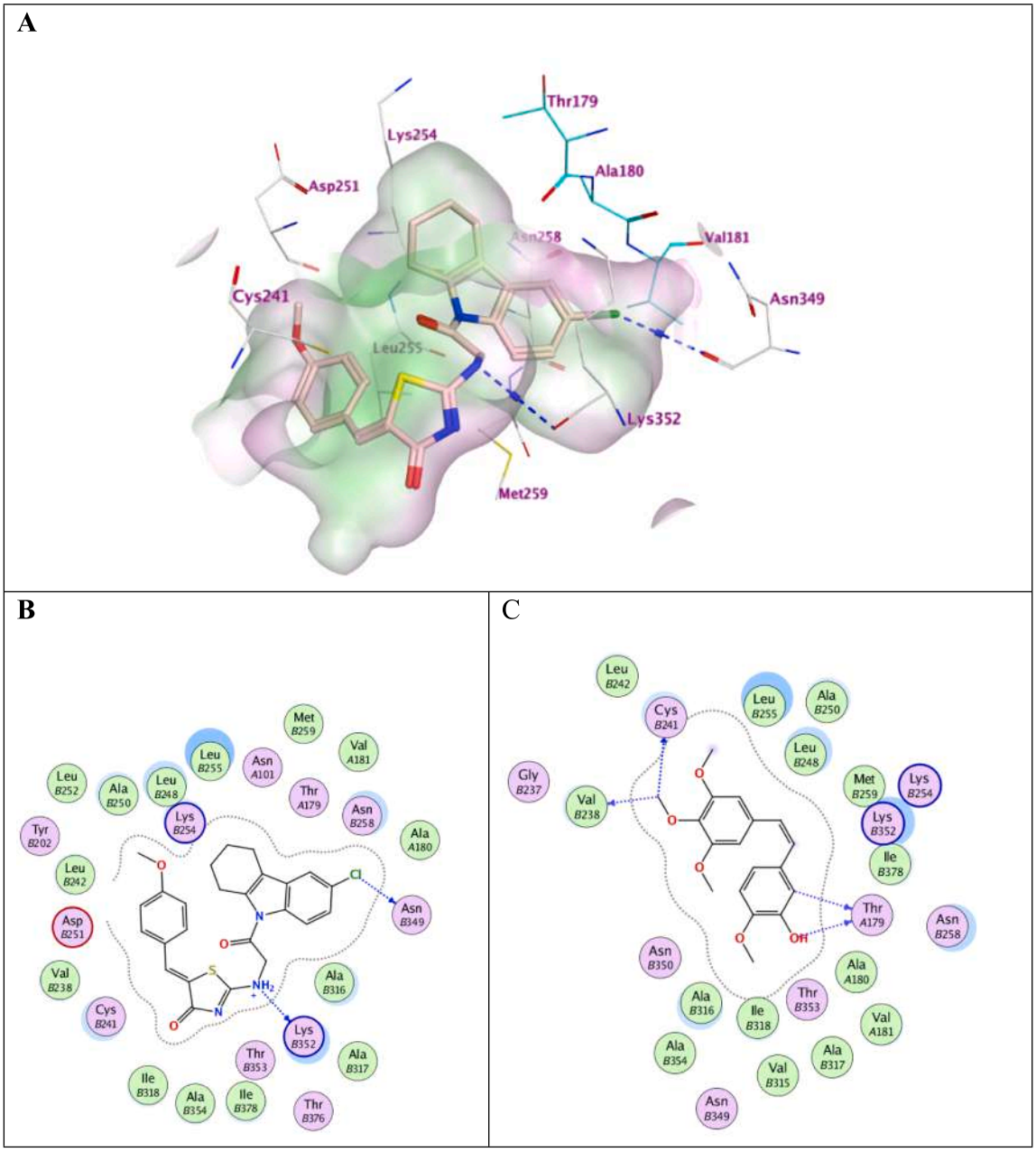

Fig. 9. Ligplots at α/β-tubulin colchicine binding site; A: 3D-docked model of compound **10g** (pink) showing the protein lipophilicity surface (purple: hydrophilic, white:neutral, Green: lipophilic), (cyan for α chain residues, white for β chain residues), B: 2D-docked model of Vinblastine. (For interpretation of the references to color in this figure legend, the reader is referred to the web version of this article.)

with their relatively higher binding affinity compared to their affinity at the vinca binding site. Moreover, SAR study summarized the binding contribution of THC linked 4-thiazolinone hybrid as well as the introduced arylidene moieties at the target proteins (Fig. 10**).**

3. Conclusion

This study proposed the design and synthesis of new anticancer compounds acting by multiple mechanisms through combining THC and 5-arylidene-4-thiazolinones. Both are privileged scaffolds exhibiting anticancer activities through multiple mechanisms. The new 20 hybrids were screened for *in vitro* antiproliferative activity against a panel of seven human cancer cell lines using an SRB assay. Among the tested compounds, **9d**, **10e**, **10f,** and **10g** showed the highest activity against leukemia with IC_{50} 3.11, 4.53, 11.89, and 5.13 μM, respectively. For the Lymphoma U937 cell line, compounds **10e**, **10f,** and **10g** showed the highest activity with IC_{50} 6.79, 6.53 and 7.31 μM, respectively. The results revealed that the antiproliferative activity improves by introducing Cl at the 6th position and electron donating substituents at the 5th position of arylidene moiety. The most active compounds **9d**, **10e**, **10f,** and **10g** are noncytotoxic to normal lymphocytes (PCS-800–017). They were evaluated for their ability as dual inhibitors of VEGFR-2 and EGFR. Compound **10e** showed a significant dual inhibitory activity against VEGFR-2 and EGFR enzyme with IC_{50} 0.26 and 0.14 μM, respectively. For tubulin polymerization enzyme assay, compounds **10e**, **10f,** and **10g** were evaluated. Compound **10g** showed a promising inhibitory activity (IC_{50} 9.95 μM) higher than vincristine. The mechanism of apoptosis was investigated by compound **10e** in Jurkat cells, and it was found that it induces apoptosis, and arrests the cell cycle at the G0-G1 phase. The compounds modes of binding with VEGFR-2, EGFR and

Table 7
Ligand-protein complex interactions of the tested compounds **9d**, **10e** and **10g** within the colchicine binding site of tubulin.

Compd.	MOE Score kcal/mol	H- bond interactions (Å)	Hydrophobic interactions	Pi-H interactions (Å)
Combretastatin	−10.16	αThr179 (3.42, 3.36)	βAsn258, βLys352, αAla316, βCys241, βLeu248, βAla250, βLeu255, βAla316,	.....
9d	−9.16	βAsp251 (3.38)	βAsn258, βLys352, αThr179, αMet259, βCys241, βLeu248, αAsn349, βAsp251	βLeu255 (3.70, 3.75)
10e	−9.06	βAsn349 (3.44)	βAsn258, βLys352, αMet259, αAla316, αAsn349, βCys241, βLeu248, βLeu255	βAla316 (4.29)
10g	−9.61	βLys352 (3.46) βAsn349 (3.46)	βAsn258, βLys352, αMet259, αAla316, αAsn349, βCys241, βLeu248, βLeu255	.....

tubulin were rationalized by molecular modeling in comparison with the co-crystalized ligands. This study suggests that hybrids **10e** and **10g** are valuable leads to hopefully develop multitarget antileukemia and antilymphoma.

4. Experimental

4.1. Chemistry

All chemicals and solvents were commercially available and used without further purification. The reactions were followed up, monitored by using aluminum-backed TLC plates (Kieselgel 0.25 mm, 60G F254, Merck, Germany) and visualized by UV light at 254 nm wavelength (Spectroline, model CM-10, USA). Melting points were determined on an electrothermal melting point apparatus (Stuart Scientific, model SM.P.3, England, UK), and were uncorrected. (IR) spectra (KBr discs) were recorded on thermo scientific nicolet IS10 FT IR spectrometer (thermo Fischer scientific, USA) at Faculty of Science, Assiut University, Assiut, Egypt. Some of the intermediates were detected by ^{1}H NMR Spectra on a Varian EM-360 L NMR spectrometer (60 MHz, Varian, CA, USA) at Faculty of Pharmacy, Assiut University, Assiut, Egypt. ^{1}H and ^{13}C NMR spectra of the final compounds were scanned on Avance-III, High performance FT-NMR spectrum, Bruker biospin international AG-Switzeraland at 400 MHz at Faculty of Science, Zagazig University, Egypt. The data were reported as chemical shifts or δ values (ppm) relative to tetramethylsilane as internal standard. Elemental microanalyses were performed by mycology and biotechnology (RCMB), faculty of science, Al-Azhar university, Nasr city, Cairo, Egypt. The tetrahydrocarbazole signals in NMR are described as THC. Single-crystal diffraction was recorded on an Agilent SuperNova Dual Atlas diffractometer using either Mo or Cu radiation. The structures were solved using SHELXT and refined by SHELXL, school of chemistry, Cardiff University, Cardiff, CF10 3AT UK.

4.1.1. General procedure for the synthesis of (Z)-5-(substituted-arylidene)-2-thioxo-4-thiazolinone (RDIa-j)

Compounds **RDIa-j** were synthesized according to the literature method [48]. Their physical and spectral data are agreed to the reported values [48,70–72].

4.1.2. General procedure for synthesis of methyl (Z)-2-[(5-(substituted-arylidene)-4-oxo-4,5-dihydrothiazol-2-yl) thio] acetate (RDIIa-j)

A solution of the appropriate **RD**Ia-j (6.32 mmol, 1 eq.) in dry acetone (15 ml) and TEA (0.9 ml, 6.32 mmol, 1 eq.) was stirred for 15 min. Methyl bromoacetate (0.7 ml, 7.59 mmol, 1.2 eq.) was added dropwise, then the reaction mixture was refluxed for 4–7 h. The

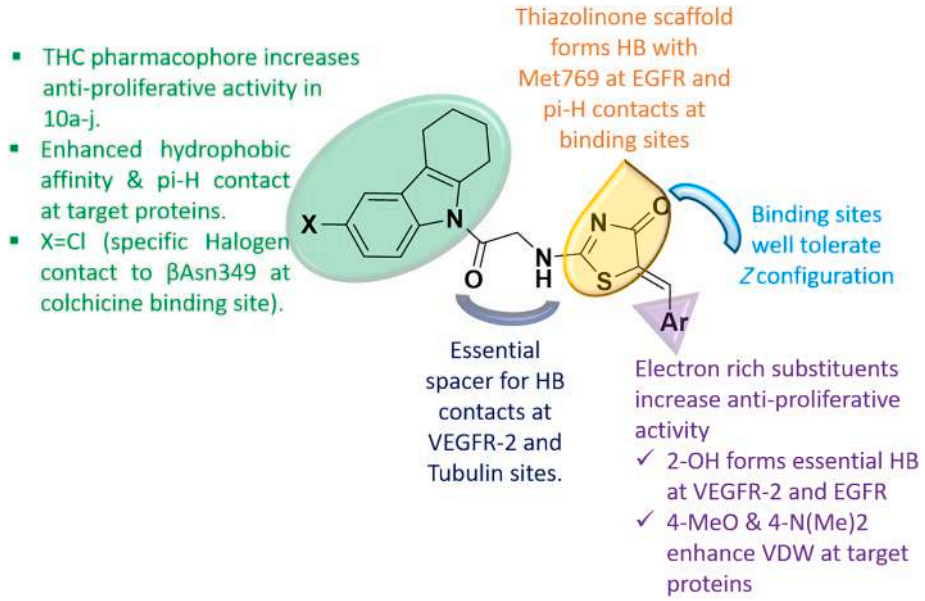

Fig. 10. Structure activity relationship of hybrids of THC and 5-arylidene-4-thiazolinone as potential anticancer.

precipitate obtained after cooling was filtered, washed with acetone, and recrystallized from ethanol to afford compounds **RD**IIa-j.

4.1.2.1. Methyl (Z)-2-((5-(4-chlorobenzylidene)-4-oxo-4,5-dihydrothiazol-2-yl) thio)acetate (RDIIa). Yield: 1.82 g (91 %); yellow solid; m.p.: 155–157 °C; IR (KBr, ύ cm^{-1}): 3107, 2960, 2930, 1736, 1701, 1613, 1472, 1147, 1105, 749, 695; ^{1}HNMR (400 MHz, DMSO-d_6) δ = 7.85 (s, 1H; =CH), 7.66 (d, *J*=8.8 Hz, 2H; ArH-3, 5), 7.60 (d, *J*=8.5 Hz, 2H; ArH-2, 6), 4.41 (s, 2H; SCH_2), 3.73 (s, 3H; CH_3O).

4.1.2.2. Methyl (Z)-2-((5-(4-bromobenzylidene)-4-oxo-4,5-dihydrothiazol-2-yl) thio)acetate (RDIIb). Yield: 2.4 g (84 %); yellow solid; m.p.: 172–174 °C; IR (KBr, ύ cm^{-1}): 2978, 2953, 2929, 1736, 1701, 1611, 1470, 1173, 1150, 749, 695; ^{1}HNMR (400 MHz, DMSO-d_6) δ = 7.54 (s, 1H; =CH), 7.38 (d, *J*=7.1 Hz, 2H; ArH-3, 5), 7.19 (d, *J*=6.9 Hz, 2H; ArH-2, 6), 4.06 (s, 2H; SCH_2), 3.54 (s, 3H; CH_3O).

4.1.2.3. Methyl (Z)-2-((5-(4-methylbenzylidene)-4-oxo-4,5-dihydrothiazol-2-yl) thio)acetate (RDIIc). Yield: 2.2 g (81 %); yellow solid; m.p.: 165–167 °C; IR (KBr, ύ cm^{-1}):2975, 2930, 1727, 1700, 1593, 1509, 1466, 1144, 976, 805, 605; ^{1}HNMR (400 MHz, DMSO-d_6) δ = 7.83 (s, 1H; =CH), 7.54 (d, *J*=7.5 Hz, 2H; ArH-2, 6), 7.36 (d, *J*=7.4 Hz, 2H; ArH-3, 5), 4.40 (s, 2H; SCH_2), 3.72 (s, 3H; CH_3O), 2.37 (s, 3H; CH_3).

4.1.2.4. Methyl (Z)-2-((5-(4-(dimethylamino)benzylidene)-4-oxo-4,5-dihydrothiazol-2-yl)thio)acetate (RDIId). Yield: 2.1 g (64 %); red solid; m.p.: 158–160 °C; IR (KBr, ύ cm^{-1}):2976, 2917, 2849, 1737, 1681, 1610, 1566, 1467, 1169, 1150, 813, 676; ^{1}HNMR (400 MHz, DMSO-d_6) δ = 7.46 (s, 1H; =CH), 7.14 (d, *J*=6.9 Hz, 2H; ArH-2, 6), 6.50 (d, *J*=6.3 Hz, 2H; ArH-3, 5), 4.01 (s, 2H; SCH_2), 3.54 (s, 3H; CH_3O), 2.82 (s, 6H; $N(CH_3)_2$).

4.1.2.5. Methyl (Z)-2-((5-(2-hydroxybenzylidene)-4-oxo-4,5-dihydrothiazol-2-yl) thio)acetate (RDIIe). Yield: 1.8 g (60 %); yellow solid; m.p.: 169–171 °C; IR (KBr, ύ cm^{-1}): 3150, 3048, 2976, 2932, 1741, 1667, 1583, 1456, 1187, 1159, 758, 634; ^{1}H NMR (400 MHz, $CDCl_3$) δ = 10.03 (brs, 1H; OH), 7.82 (s, 1H; =CH), 6.93–6.77 (m, 2H; ArH), 6.56–6.43 (m, 2H; ArH), 3.83 (s, 2H; SCH_2), 3.33 (s, 3H; CH_3O).

4.1.2.6. Methyl (Z)-2-((5-(4-hydroxybenzylidene)-4-oxo-4,5-dihydrothiazol-2-yl) thio)acetate (RDIIf). Yield: 2.1 g (70 %); yellow solid; m.p.: 198–200 °C; IR (KBr, ύ cm^{-1}): 3138 (br), 3049, 2959, 1728, 1677, 1584, 1449, 1153, 989, 704. ^{1}H NMR (400 MHz, DMSO-d_6) δ = 10.50 (brs, 1H; OH), 7.77 (s, 1H; =CH), 7.52 (d, *J*=7.5 Hz, 2H; ArH-2, 6), 6.93 (d, *J*=7.2 Hz, 2H; ArH-3, 5), 4.36 (s, 2H; SCH_2), 3.70 (s, 3H; CH_3O).

4.1.2.7. Methyl (Z)-2-((5-(4-methoxybenzylidene)-4-oxo-4,5-dihydrothiazol-2-yl) thio)acetate (RDIIg). Yield: 2.88 g (93 %); yellow solid; m.p.: 160–162 °C; IR (KBr, ύ cm^{-1}): 3110, 2982, 2859, 1745, 1701, 1585, 1508, 1458, 1150, 979, 775. ^{1}H NMR (400 MHz, DMSO-d_6) δ = 7.83 (s, 1H; =CH), 7.63 (d, *J*=8.5 Hz, 2H; ArH-2, 6), 7.12 (d, *J*=8.3 Hz, 2H; ArH-3, 5), 4.42 (s, 2H; SCH2), 3.85 (s, 3H; CH_3O), 3.72 (s, 3H; CH_3O).

4.1.2.8. Methyl (Z)-2-((5-(3,4-dimethoxybenzylidene)-4-oxo-4,5-dihydrothiazol-2-yl)thio)acetate (RDIIh). Yield: 2.8 g (80 %); yellow solid; m.p.: 135–136 °C; IR (KBr, ύ cm^{-1}): 2938, 2834, 1727, 1694, 1576, 1468, 1156, 1131, 837; ^{1}H NMR (60 MHz, $CDCl_3$) δ = 7.85 (s, 1H; =CH), 7.35–6.85 (m, 3H; ArH-2, 5, 6), 4.35 (s, 2H; SCH_2), 4.00 (s, 6H; CH_3O), 3.85 (s, 3H; CH_3O).

4.1.2.9. Methyl (Z)-2-((4-oxo-5-(3,4,5-trimethoxybenzylidene)-4,5-dihydrothiazol-2-yl) thio)acetate (RDIIi). Yield: 2.8 g (74 %); yellow solid; m.p.: 157–159 °C; IR (KBr, ύ cm^{-1}): 2975, 2938, 2837, 1727, 1596, 1504, 1463, 1190, 1170, 748, 631; ^{1}HNMR (400 MHz, DMSO-d_6) δ = 7.78 (s, 1H; =CH), 6.93 (s, 2H; ArH-2, 6), 4.36 (s, 2H; SCH_2), 3.83 (s, 6H; CH_3O), 3.73 (s, 3H; CH_3O), 3.70 (s, 3H; CH_3O).

4.1.2.10. Methyl 2-(((Z)-4-oxo-5-((E)-3-phenylallylidene)-4,5-dihydrothiazol-2-yl) thio)acetate (RDIIj). Yield: 2.1 g (69 %); yellow solid; m.p.: 156–158 °C; IR (KBr, ύ cm^{-1}): 3001, 2954, 2918, 2851, 1732, 1689, 1606, 1580, 1456, 1199, 1142, 757, 688; ^{1}HNMR (400 MHz, DMSO-d_6) δ = 7.20–7.16 (m, 3H; ArH-2, 6, =CH-CH=CH), 7.05–7.00 (m, 3H; ArH-3, 4, 5), 6.78 (d, *J*=15.2 Hz, 1H; =CH-CH=CH), 6.45 (dd, *J*=15.1, 11.4 Hz, 1H; =CH-CH=CH), 3.89 (s, 2H; SCH_2), 3.41 (s, 3H; CH_3O).

4.1.3. Synthesis of 4-chlorophenylhydrazine hydrochloride (2)

Phenylhydrazine hydrochloride 1 was commercially available, while 4-chlorophenyl hydrazine hydrochloride 2 was synthesized according to the literature method [54].

4.1.4. General procedure for the synthesis of THC or 6-chloroTHC (3 and 4)

Compounds **3**, and **4** were synthesized according to the reported method [50]. Their physical and Spectral data were agreed to those previously reported values [51–53].

4.1.5. General procedure for the synthesis of 2-bromo-1-(6-chloro or unsubstituted 1,2,3,4-tetrahydro-9H-carbazol-9-yl) ethan-1-one (5 and 6)

To the appropriate stirred solution of THC or 6-chloroTHC (3 or 4) (5 g, 29.2 mmol) in chloroform (10 ml), bromoacetyl bromide (5.8 mmol, 2 eq.) was added dropwise. The mixture was refluxed for 7 h until completion of the reaction, cooled, evaporated under vacuum, and finally recrystallized from ethanol to give the bromoacetamide compounds 5 or 6, respectively.

4.1.5.1. Bromo-1-(1,2,3,4-tetrahydro-9H-carbazol-9-yl) ethan-1-one (5). Yield: 6.2 g (73 %); white solid; m.p.: 141–143 °C; IR (KBr, ύ cm^{-1}): 3080, 3068, 3012, 2949, 2932, 2887, 2861, 2843, 1714, 1616, 1474, 954, 768; ^{1}H NMR (60 MHz, $CDCl_3$) δ = 8.05 (dd, *J*=8.1, 2.7 Hz, 1H; ArH-8 THC), 7.45–7.05 (m, 3H; ArH-5, 6, 7 THC), 4.35 (s, 2H; CH_2Br), 2.95 (t, *J*=7.2 Hz, 2H; H-1 THC), 2.60 (t, *J*=7.1 Hz, 2H; H-4 THC), 2.05–1.65 (m, 4H; H-2, 3 THC).

4.1.5.2. Bromo-1-(6-chloro-1,2,3,4-tetrahydro-9H-carbazol-9-yl) ethan-1-one (6). Yield: 5.8 g (74 %); white solid; m.p.: 137–139 °C; IR (KBr, ύ cm^{-1}): 3064, 3043, 2951, 2940, 2931, 2879, 2863, 1698, 1613, 1462, 1444, 1132, 1077, 861, 708, 689; ^{1}HNMR (400 MHz, DMSO-d_6) δ = 8.00 (d, *J*=8.8 Hz, 1H; ArH-8 THC), 7.26–7.09 (m, 2H; ArH-5, 7 THC), 4.44 (s, 2H; CH_2Br), 3.97 (brs, 2H; H-1 THC), 2.94 (brs, 2H; H-4 THC), 1.97–175 (m, 4H; H-2, 3 THC).

4.1.6. General procedure for the synthesis of 2-amino-1-(6-chloro or unsubstituted 1,2,3,4-tetrahydro-9H-carbazol-9-yl) ethan-1-one (7 and 8)

To a solution of the appropriate bromoacetamide **5** or **6** (5 g, 1 eq.) dissolved in chloroform (30 ml), hexamethylenetetramine (2.9 g, 1.1 eq.) was added. The reaction was refluxed for 5 h at 60 °C. The white precipitate obtained was filtered, washed with chloroform, and dried. The obtained HBr salt then dissolved in 10 ml ethanol, and 5 ml HCl by dropwise addition. After stirring for 18 h at room temperature, the white precipitate was filtered and washed with ethanol to afford compounds 7 or 8, respectively.

4.1.6.1. 2-Amino-1-(1,2,3,4-tetrahydro-9H-carbazol-9-yl) ethan-1-one hydrochloride (7). Yield: 3.3 g (81 %); white solid; m.p.: 271–273 °C; IR (KBr, ύ cm^{-1}): 3369, 3047, 2932, 2855, 1694, 1612, 1578, 1455, 804, 745; ^{1}HNMR (400 MHz, DMSO-d_6) δ = 8.17 (dd, *J*=6.7, 2.1 Hz, 1H; ArH-8 THC), 7.62–7.24 (m, 6H; ArH-5, 6, 7 THC, NH_2HCl), 4.47 (s, 2H; CH_2NH_3), 2.94 (t, *J*=6.8 Hz, 2H; H-1 THC), 2.58 (t, *J*=6.9 Hz, 2H; H-4 THC), 1.86–1.70 (m, 4H; H-2, 3 THC).

4.1.6.2. 2-Amino-1-(6-chloro-1,2,3,4-tetrahydro-9H-carbazol-9-yl)ethan-1-one hydrochloride (8). Yield: 3.8 g (82 %); white solid; m.p.: 260–262 °C; IR (KBr, ύ cm^{-1}): 3224, 3161, 3037, 2953, 1691, 1655, 1614, 1459, 1425, 955, 812; ^{1}HNMR (400 MHz, DMSO-d_6) δ = 8.21 (d, *J*=8.8 Hz, 1H; ArH-8 THC), 7.54–7.30 (m, 5H; ArH-5, 7 THC, NH_2HCl), 4.48 (s, 2H; CH_2NH_3), 2.96 (t, *J*=7.2 Hz, 2H; H-1 THC), 2.59 (t, *J*=6.8 Hz, 2H; H-4 THC), 1.88–1.72 (m, 4H; H-2, 3 THC).

4.1.7. General procedure for the synthesis of the target compounds ***9a-j*** *and* ***10a-j***

To a stirred solution of compounds 7or 8 (0.2 g, 0.755 mmol) in absolute ethanol (10 ml) and TEA (0.11 ml, 1 eq) and the appropriate rhodanine derivative **RD**IIa-j (1 eq) was added. The solution was refluxed for 5–11 h until the completion of the reaction (TLC monitoring), then the obtained solid was filtered, washed with hot ethanol, and recrystallized from DMSO/H_2O (9:1).

4.1.7.1. (Z)-5-(4-Chlorobenzylidene)-2-((2-oxo-2-(1,2,3,4-tetrahydro-9H-carbazol-9-yl) ethyl)amino)-thiazol-4(5H)-one (9a). Yield: 113 mg (33 %); Yellow solid; m.p.: 230–231 °C; IR (KBr, ύ cm^{-1}): 3203, 2939, 2858, 1691, 1616, 1573, 1558, 965, 816, 745, 637; ^{1}H NMR (400 MHz, DMSO-d_6) δ = 10.27 (brs, 1H; NH), 8.18 (d, *J*=7.1 Hz, 1H; ArH-8 THC), 7.66–7.58 (m, 5H; ArH-2′, 3′, 5′, 6′, =CH), 7.47 (d, *J*=7.9 Hz, 1H; ArH-5 THC), 7.31–7.26 (m, 2H; ArH-6, 7 THC), 5.08 (s, 2H; CH_2NH), 3.03 (brs, 2H; H-1 THC), 2.63 (brs, 2H; H-4 THC), 192–1.76 (m, 4H; H-2, 3 THC); ^{13}C NMR (100 MHz, DMSO-d_6) δ = 179.2, 174.4, 167.9, 135.4, 134.5, 134.2, 132.9, 131.1, 129.8, 129.5, 129.3, 128.5, 124.3, 123.4, 118.2, 117.9, 115.8, 49.5, 25.7, 23.3, 21.3, 20.7; Analysis calc. for $C_{24}H_{20}ClN_3O_2S$ (449.95):C, 64.06; H, 4.48; N, 9.34; S, 7.13. Found: C, 64.21; H, 4.59; N, 9.53; S, 7.32.

4.1.7.2. (Z)-5-(4-Bromobenzylidene)-2-((2-oxo-2-(1,2,3,4-tetrahydro-9H-carbazol-9-yl) ethyl)amino)-thiazol-4(5H)-one (9b). Yield: 195 mg (53 %); White crystal; m.p.: 237–239 °C; IR (KBr, ύ cm^{-1}): 3180, 3161, 3047, 2942, 2856, 2846, 1701, 1606, 1564, 1555, 1486, 984, 951, 934, 754, 735; ^{1}H NMR (400 MHz, DMSO-d_6) δ = 10.27 (brs, 1H; NH), 8.18 (dd, *J*=6.8, 3.2 Hz, 1H; ArH-8 THC), 7.73 (d, *J*=8.4 Hz, 2H; ArH-3′, 5′), 7.60 (s, 1H; =CH), 7.53 (d, *J*=8.5 Hz, 2H; ArH-2′, 6′), 7.48–7.45 (m, 1H; ArH-5 THC), 7.31–7.24 (m, 2H; ArH-6, 7 THC), 5.07 (s, 2H; CH_2NH), 3.03 (t, *J*=6.6 Hz, 2H; H-1 THC), 2.63 (t, *J*=6.7 Hz, 2H; H-4 THC), 1.92–1.75 (m, 4H; H-2, 3 THC); ^{13}C NMR (100 MHz, DMSO-d_6) δ = 179.2, 174.4, 167.9, 135.4, 134.5, 133.3, *132.23*, *132.15*, 131.3, 129.8, 129.6, 128.6, 124.2, 123.4, 118.2, 117.9, 115.8, 49.5, 25.6, 23.3, 21.3, 20.7; Analysis calc. for $C_{24}H_{20}BrN_3O_2S$ (494.40): C, 58.30; H, 4.08; N, 8.50; S, 6.49. Found: C, 58.54; H, 4.21; N, 8.74; S, 6.56.

4.1.7.3. (Z)-5-(4-Methylbenzylidene)-2-((2-oxo-2-(1,2,3,4-tetrahydro-9H-carbazol-9-yl)ethyl)amino)-thiazol-4(5H)-one (9c). Yield: 155 mg (48 %); white solid; m.p.: 257–258 °C; IR (KBr, ύ cm^{-1}): 3216, 3120, 3021, 2934, 2858, 1698, 1678, 1618, 1604, 1572, 1516, 950, 804, 761, 638; ^{1}H NMR (400 MHz, DMSO-d_6) δ = 10.17 (t, *J*=5.8 Hz, 1H; NH), 8.18 (dd, *J*=6.9, 2.7 Hz, 1H; ArH-8 THC), 7.59 (s, 1H; =CH), 7.51–7.46 (m, 3H; ArH-5 THC, ArH-2′, 6′), 7.35 (d, *J*=8.1 Hz, 2H; ArH-3′, 5′), 7.32–7.25 (m, 2H; ArH-6, 7 THC), 5.03 (s, 2H; CH_2NH), 3.03 (t, *J*=7.1 Hz, 2H; H-1 THC), 2.64 (t, *J*=6.8 Hz, 2H; H-4 THC), 2.36 (s, 3H; CH_3), 1.92–1.77 (m, 4H; H-2, 3 THC); ^{13}C NMR (100 MHz, DMSO-d_6) δ = 179.5, 174.7, 168.0, 139.9, 135.4, 134.6, 131.2, 130.0, 129.9, 129.9, 129.6, 127.5, 124.3, 123.5, 118.2, 117.9, 115.8, 49.4, 25.7, 23.3, 21.3, 21.1, 20.7; Analysis calc. for $C_{25}H_{23}N_3O_2S$ (429.53): C, 69.91; H, 5.40; N, 9.78; S, 7.47. Found: C, 70.12; H, 5.62; N, 9.97; S, 7.60.

4.1.7.4. (Z)-5-(4-(Dimethylamino)benzylidene)-2-((2-oxo-2-(1,2,3,4-tetrahydro-9H-carbazol-9-yl) ethyl)amino)-thiazol-4(5H)-one (9d). Yield: 191 mg (55 %); Yellow solid; m.p.: 274–276 °C; IR (KBr, ύ cm^{-1}): 3217, 3029, 2920, 2855, 1692, 1667, 1593, 1520, 961, 808, 632; ^{1}H NMR (400 MHz, DMSO-d_6) δ = 9.98 (t, *J*=5.7 Hz, 1H; NH), 8.18 (dd, *J*=6.7, 2.8 Hz, 1H; ArH-8 THC), 7.52 (s, 1H; =CH), 7.46 (dd, *J*=6.5, 2.9 Hz, 1H; ArH-5 THC), 7.42 (d, *J*=8.6 Hz, 2H; ArH- 2′, 6′), 7.32–7.24 (m, 2H; ArH-6, 7 THC), 6.82 (d, *J*=8.7 Hz, 2H; ArH-3′, 5′), 5.03 (d, *J*=5.2 Hz, 2H; CH_2NH), 3.06–2.97 (m, 8H; H-1THC, $N(CH_3)_2$), 2.63 (t, *J*=6.9 Hz, 2H; H-4 THC), 1.92–1.76 (m, 4H; H-2, 3 THC); ^{13}C NMR (100 MHz, DMSO-d_6) δ = 179.9, 174.3, 168.2, 151.0, 135.4, 134.6, 131.3, 131, 129.8, 124.2, 123.4, 121.8, 120.8, 118.1, 117.9, 115.8, 112.1, 49.2, 40.4, 25.67, 23.3, 21.3, 20.7; Analysis calc. for $C_{26}H_{26}N_4O_2S$ (458.58): C, 68.10; H, 5.71; N, 12.22; S, 6.99. Found: C, 68.32; H, 5.85; N, 12.49; S, 7.08.

4.1.7.5. (Z)-5-(2-Hydroxybenzylidene)-2-((2-oxo-2-(1,2,3,4-tetrahydro-9H-carbazol-9-yl) ethyl)amino)-thiazol-4(5H)-one (9e). Yield: 93 mg (19 %); yellow solid; m.p.: 186–188 °C; IR (KBr, ύ cm^{-1}): 3586, 3227, 3042, 3010, 2929, 2860, 1698, 1675, 1601, 1555, 1512, 1496, 986, 964, 950, 761, 745, 734; ^{1}H NMR (400 MHz, DMSO-d_6) δ = 10.32 (brs, 1H; OH), 10.12 (brs, 1H; NH), 8.18 (dd, *J*=6.6, 1.9 Hz, 1H; ArH-8 THC), 7.91 (s, 1H; =CH), 7.47 (dd, *J*=6.1, 2.4 Hz, 1H; ArH-5 THC), 7.38 (d, *J*=7.6 Hz, 1H; ArH-7 THC), 7.32–7.24 (m, 3H; ArH-6 THC, Ar'H), 6.99–6.94 (t, *J*=7.9 Hz, 2H; Ar'H), 5.06 (s, 2H; CH_2NH), 3.03 (t, *J*=7.2 Hz, 2H; H-1 THC), 2.63 (t, *J*=6.9 Hz, 2H; H-4 THC), 1.93–1.75 (m, 4H; H-2, 3 THC); ^{13}C NMR (100 MHz, DMSO-d_6) δ = 180.0, 175.3, 168.5, 157.4, 135.9, 135.1, 131.8, 130.3, 128.3, 127.8, 125.5, 124.7, 123.9, 121.4, 120.1, 118.6, 118.4, 116.5, 116.3, 49.8, 26.12, 23.7, 21.8, 21.2; Analysis calc. for $C_{24}H_{21}N_3O_3S$ (431.51): C, 66.80; H, 4.91; N, 9.74; S, 7.43. Found: C, 67.11; H, 5.07; N, 9.86; S, 7.52.

4.1.7.6. (Z)-5-(4-Hydroxybenzylidene)-2-((2-oxo-2-(1,2,3,4-tetrahydro-9H-carbazol-9-yl)ethyl)amino)-thiazol-4(5H)-one (9f). Yield: 110 mg (33 %); yellow solid; m.p.: 239–240 °C; IR (KBr, ύ cm^{-1}): 3299, 3218, 3031, 2938, 2858, 1688, 1673, 1600, 1580, 1511, 1475, 986, 950, 867, 755, 632; ^{1}H NMR (400 MHz, DMSO-d_6) δ = 10.19 (brs, 1H; OH), 10.09 (brs, 1H; NH), 8.17 (brs, 1H; ArH-8 THC), 7.54 (s, 1H; =CH), 7.49–7.37 (m, 3H; ArH-5 THC, ArH-2′, 6′), 7.27 (brs, 2H; ArH-6, 7 THC), 6.91 (d, *J*=7.6 Hz, 2H; ArH-3′, 5′), 5.04 (s, 2H; CH_2NH), 3.02 (brs, 2H; H-1 THC), 2.63 (brs, 2H; H-4 THC), 1.96–1.72 (m, 4H; H-2, 3 THC);^{13}C NMR (100 MHz, DMSO-d_6) δ = 179.8, 174.7, 168.1, 159.2, 135.1, 134.6,131.7, 130.4, 129.9, 124.8, 124.6, 124.3, 123.5, 118.2, 118.0, 116.3, 115.8, 49.3, 25.7, 23.4, 21.4, 20.8; Analysis calc. for $C_{24}H_{21}N_3O_3S$ (431.51): C, 66.80; H, 4.91; N, 9.74; S, 7.43. Found: C, 66.98; H, 4.78; N, 10.02; S, 7.57.

4.1.7.7. (Z)-5-(4-Methoxybenzylidene)-2-((2-oxo-2-(1,2,3,4-tetrahydro-9H-carbazol-9-yl) ethyl)amino)-thiazol-4(5H)-one (9g). Yield: 150 mg (45 %); yellow solid; m.p.: 240–242 °C; IR (KBr, ύ cm^{-1}): 3219, 3116, 3030, 2931, 2843, 1697, 1672, 1602, 1573, 1509, 1475, 1456, 996, 950, 894, 758, 636; ^{1}HNMR (400 MHz, DMSO-d_6) δ = 10.13 (t, *J*=5.0 Hz, 1H; NH), 8.18 (dd, *J*=6.7, 2.9 Hz, 1H; ArH-8 THC), 7.59 (s, 1H; =CH), 7.55 (d, *J*=8.6 Hz, 2H; ArH-2′, 6′), 7.46 (dd, *J*=6.5, 2.9 Hz, 1H; ArH-5 THC), 7.32–7.24 (m, 2H; ArH-6, 7 THC), 7.11 (d, *J*=8.7 Hz, 2H; ArH-3′, 5′), 5.06 (d, *J*=5.5 Hz, 2H; CH_2NH), 3.82 (s, 3H; CH_3O), 3.03 (t, *J*=7.2 Hz, 2H; H-1 THC), 2.63 (t, *J*=7.1 Hz, 2H; H-4 THC), 1.93–1.75 (m, 4H; H-2, 3 THC); ^{13}CNMR (100 MHz, DMSO-d_6) δ = 179.8, 174.8, 168.1, 160.6, 135.5, 134.7, 131.5, 130.1, 130.0, 126.4, 125.8, 124.4, 123.6, 118.3, 118.1, 115.9, 114.9, 55.6, 49.4, 25.8, 23.4, 21.4, 20.8; Analysis calc. for $C_{25}H_{23}N_3O_3S$ (445.5): C, 67.40; H, 5.20; N, 9.43: S, 7.20. Found: C, 67.67; H, 5.39; N, 9.65; S, 7.31.

4.1.7.8. (Z)-5-(3,4-Dimethoxybenzylidene)-2-((2-oxo-2-(1,2,3,4-tetrahydro-9H-carbazol-9-yl) ethyl)amino)-thiazol-4(5H)-one (9h). Yield: 140 mg (38 %); yellow solid; m.p.: 215–217 °C; IR (KBr, ύ cm^{-1}): 3201, 3005,

2933, 1697, 1685, 1608, 1594, 1535, 1509, 1455, 949, 766, 796, 676; ^{1}HNMR (400 MHz, DMSO-d_6) δ = 10.11 (t, *J*=5.5 Hz, 1H; NH),

8.18 (d, *J*=7.9 Hz, 1H; ArH-8 THC), 7.60 (s, 1H; =CH), 7.46 (d, *J*=6.1 Hz, 1H; ArH-5 THC), 7.32–7.12 (m, 5H; ArH-6, 7 THC, Ar'H), 5.05 (d, *J*=5.5 Hz, 2H; CH_2NH), 3.82 (s, 6H; CH_3O), 3.03 (t, *J*=6.9 Hz, 2H; H-1 THC), 2.63 (t, *J*=6.6 Hz, 2H; H-4 THC), 1.92–1.76 (m, 4H; H-2, 3 THC); ^{13}CNMR(100 MHz, DMSO- d_6) δ = 180.0, 175.0, 168.5, 150.7, 149.4, 135.9, 135.0, 130.7, 130.3, 127.1, 126.4, 124.7, 123.9, 123.3, 118.6, 118.4, 116.3, 113.5, 112.6, 56.1, 56, 49.8, 26.1, 23.8, 21.8, 21.2; Analysis calc. for $C_{26}H_{25}N_3O_4S$ (475.56): C, 65.67; H, 5.30; N, 8.84; S, 6.74. Found: C, 65.85; H, 5.41; N, 9.07; S, 6.81.

4.1.7.9. (Z)-5-(3,4,5-Trimethoxybenzylidene)-2-((2-oxo-2-(1,2,3,4-tetrahydro-9H-carbazol-9-yl)ethyl)amino)-thiazol-4(5H)-one (9i). Yield: 206 mg (54 %); white solid; m.p.: 173–175 °C; IR (KBr, ύ cm^{-1}): 3138, 2992, 2935, 2857, 1700, 1611, 1581, 1561, 1448, 1420, 1403, 952, 822, 753, 632; ^{1}HNMR (400 MHz, DMSO-d_6) δ = 10.18 (brs, 1H; NH), 8.17 (dd, *J*=6.9, 1.9 Hz; 1H, ArH-8 THC), 7.59 (s, 1H; =CH), 7.46 (dd, *J*=6.5, 2.2 Hz, 1H; ArH-5 THC), 7.30–7.24 (m, 2H; ArH-6, 7 THC), 6.93 (s, 2H; ArH-2′, 6′), 5.06 (brs, 2H; CH_2NH), 3.85 (s, 6H; CH_3O), 3.73 (s, 3H; CH_3O), 3.02 (t, *J*=7.1 Hz, 2H; H-1 THC), 2.64 (t, *J*=6.6 Hz, 2H; H-4 THC), 1.91–1.75 (m, 4H; H-2, 3 THC); ^{13}CNMR(100 MHz, DMSO-d_6)δ = 179.4, 174.6, 167.9, 153.2, 138.8, 135.4, 134.6, 130.2, 129.8, 129.6, 127.8, 124.3, 123.5, 118.2, 117.9, 115.8, 107.1, 60.23, 56.0, 49.4, 40.2, 25.7, 23.3, 21.3, 20.7; Analysis calc. for $C_{27}H_{27}N_3O_5S$ (505.5): C, 64.14; H, 5.38; N, 8.31; S, 6.34. Found: C, 64.40; H, 5.52; N, 8.49; S, 6.41.

4.1.7.10. (Z)-5-((E)-3-Phenylallylidene)-2-((2-oxo-2-(1,2,3,4-tetrahydro-9H-carbazol-9-yl)ethyl)amino)-thiazol-4(5H)-one (9j). Yield: 120 mg (36 %); yellow crystal; m.p.: 215–217 °C; IR (KBr, ύ cm^{-1}): 3188, 3021, 2928, 2855, 1701, 1601, 1589, 1556, 1489, 960, 841, 743, 690, 677, 634; ^{1}HNMR (400 MHz, DMSO-d_6) δ = 10.11 (brs, 1H; NH), 8.19 (dd, *J*=6.7, 2.8 Hz, 1H; ArH-8 THC), 7.65 (d, *J*=7.4 Hz, 2H; ArH-2′, 6′), 7.46 (dd, *J*=6.7, 2.6 Hz, 1H; ArH-5 THC), 7.43–7.26 (m, 6H; ArH-6, 7 THC, ArH-3′, 4′, 5′, =CH-CH=CH), 7.17 (d, *J*=15.2 Hz, 1H, =CH-CH=CH), 6.96 (dd, *J*=15.2, 11.3 Hz, 1H, =CH-CH=CH), 5.03 (s, 2H; CH_2NH), 3.02 (brs, 2H; H-1 THC), 2.63 (brs, 2H; H-4 THC),1.95–1.72 (m, 4H; H-2, 3 THC); ^{13}CNMR (100 MHz, DMSO-d_6) δ = 178.9, 173.9, 168.0, 141.2, 135.9, 135.4, 134.5, 131.1, 129.8, 129.6, 129.2, 128.8, 127.5, 125.2, 124.2, 123.4, 118.1, 117.9, 115.8, 49.2, 25.6, 23.3, 21.3, 20.7; Analysis calc. for $C_{26}H_{23}N_3O_2S$ (441.54): C, 70.72; H, 5.25; N, 9.52; S, 7.26. Found: C, 70.85; H, 5.42; N, 9.80; S, 7.48.

4.1.7.11. (Z)-5-(4-Chlorobenzylidene)-2-((2-(6-chloro-1,2,3,4-tetrahydro-9H-carbazol-9-yl)-2-oxoethyl)amino)-thiazol-4(5H)-one (10a). Yield: 110 mg (34 %); yellow solid; m.p.: 160–162 °C; IR (KBr, ύ cm^{-1}): 3233, 2937, 2859, 1692, 1677, 1613, 1571, 1489, 984, 971, 961, 820, 702, 637; ^{1}HNMR (400 MHz, DMSO-d_6) δ = 10.27 (brs, 1H; NH), 8.20 (d, *J*=8.8 Hz, 1H; ArH-8 THC), 7.62 (s, 1H; =CH), 7.60 (brs, 4H; ArH-2′, 3′, 5′, 6′), 7.53 (d, *J*=1.8 Hz, 1H; ArH- 5 THC), 7.30 (dd, *J*=8.9, 1.9 Hz, 1H; ArH-7 THC), 5.06 (s, 2H; CH_2NH), 3.04 (t, *J*=7.1 Hz, 2H; H-1 THC), 2.62 (t, *J*=6.8 Hz, 2H; H-4 THC), 1.91–1.75 (m, 4H; H-2, 3 THC);^{13}CNMR (100 MHz, DMSO-d_6) δ = 179.6, 174.9, 168.4, 136.7, 134.7, 134.5, 133.4, 131.8, 131.6, 129.9, 129.8, 129.1, 128.3, 124.3, 118.1, 118.0, 117.8, 49.9, 26.1, 23.6, 21.6, 21.0; Analysis calc. for $C_{24}H_{19}Cl_2N_3O_2S$ (484.4): C, 59.51; H, 3.95; N, 8.67; S, 6.62. Found: C, 59.73; H, 4.03; N, 8.90; S, 6.74.

4.1.7.12. (Z)-5-(4-Bromobenzylidene)-2-((2-(6-chloro-1,2,3,4-tetrahydro-9H-carbazol-9-yl)-2-oxoethyl) amino)-thiazol-4(5H)-one (10b). Yield: 146 mg (42 %); white solid; m.p.: 259–260 °C; IR (KBr, ύ cm^{-1}):3203, 3078, 2999, 2929, 2920, 2853, 1689, 1615, 1573, 1552, 1510, 1485, 983, 968, 815, 700, 634; ^{1}HNMR (400 MHz, DMSO-d_6):10.19 (brs, 1H; NH), 8.20 (d, *J*=8.8 Hz, 1H; ArH-8 THC), 7.75 (d, *J*=8.4 Hz, 2H; ArH-3′, 5′), 7.61 (s, 1H; =CH), 7.56–7.52 (m, 3H; ArH-5 THC, ArH-2′, 6′), 7.31 (dd, *J*=8.8, 2.2 Hz, 1H; ArH-7 THC), 5.07 (s, 2H; CH_2NH), 3.04 (t, *J*=6.9 Hz, 2H; H-1 THC), 2.63 (t, *J*=7.2 Hz, 2H; H-4 THC), 1.92–1.75 (m, 4H; H-2, 3 THC); Analysis calc. for $C_{24}H_{19}BrClN_3O_2S$ (528.85):C, 54.51; H, 3.62; N, 7.95; S, 6.06. Found: C, 54.75; H, 3.80; N, 8.12; S, 6.13.

4.1.7.13. (Z)-5-(4-Methylbenzylidene)-2-((2-(6-chloro-1,2,3,4-tetrahydro-9H-carbazol-9-yl)-2-oxoethyl) amino)-thiazol-4(5H)-one (10c). Yield: 160 mg (52 %); yellow solid; m.p.: 254–256 °C; IR (KBr, ύ cm^{-1}): 3215, 3071, 3020, 2934, 2916, 2876, 2852, 1707, 1687, 1674, 1614, 1604, 1560, 1466, 949, 896, 807, 769, 638; ^{1}HNMR (400 MHz, DMSO-d_6) δ = 10.18 (brs, 1H; NH), 8.20 (d, *J*=8.8 Hz, 1H; ArH-8 THC), 7.61 (s, 1H; =CH), 7.55 (d, *J*=1.9 Hz, 1H; ArH-5 THC), 7.49 (d, *J*=8.2 Hz, 2H; ArH-2′, 6′), 7.36 (d, *J*=7.9 Hz, 2H; ArH-3′, 5′), 7.31 (dd, *J*=8 0.7,2.1 Hz, 1H; ArH-7 THC), 5.06 (s, 2H; CH_2NH), 3.05 (t, *J*=7.2 Hz, 2H; H-1 THC), 2.63 (t, *J*=6.9 Hz, 2H; H-4 THC), 2.37 (s, 3H; CH_3), 1.93–1.77 (m, 4H; H-2, 3 THC); Analysis calc. for $C_{25}H_{22}ClN_3O_2S$ (463.97):C, 64.72; H, 4.78; N, 9.06; S, 6.91. Found: C, 64.51; H, 5.01; N, 9.28; S, 6.97.

4.1.7.14. (Z)-5-(4-Dimethylaminobenzylidene)-2-((2-(6-chloro-1,2,3,4-tetrahydro-9H-carbazol-9-yl)-2-oxoethyl) amino)-thiazol-4(5H)-one (10d). Yield: 153 mg (44 %); yellow solid; m.p.: 275–277 °C; IR (KBr, ύ cm^{-1}): 3220, 3024, 2947, 2915, 2856, 1698, 1667, 1593, 1521, 1461, 955, 815, 759, 633; ^{1}HNMR (400 MHz, DMSO-d_6) δ = 9.97 (t, *J*=5.1 Hz, 1H; NH), 8.19 (d, *J*=8.8 Hz, 1H; ArH-8 THC), 7.52 (s, 1H; =CH), 7.51 (d, *J*=2.5 Hz, 1H; ArH-5 THC), 7.41 (d, *J*=8.8 Hz, 2H; ArH-2′, 6′), 7.28 (dd, *J*=8.8, 1.9 Hz, 1H; ArH-7 THC), 6.81 (d, *J*=8.8 Hz, 2H; ArH-3′, 5′), 5.01 (d, *J*=5.5 Hz, 2H; CH_2NH), 3.05–3.01 (m, 2H; H-1 THC), 2.99 (s, 6H; N $(CH_3)_2$), 2.61 (t, *J*=6.6 Hz, 2H; H-4 THC), 1.91–175 (m, 4H; H-2, 3 THC); ^{13}C NMR (100 MHz, DMSO-d_6) δ = 179.5, 175.2, 168.3, 136.8, 134.5, 133.9, 132.6, 131.9, 131.7, 130.3, 129.1, 128.4, 124.2, 123.4, 118.1, 117.9, 117.6, 49.9, 41.1, 26.1, 23.6, 21.7, 21.0; Analysis calc. for $C_{26}H_{25}ClN_4O_2S$ (493.02): C, 63.34; H, 5.11; N, 11.36; S, 6.50. Found: C, 63.57; H, 5.08; N, 11.62; S, 6.58.

4.1.7.15. (Z)-5-(2-Hydroxybenzylidene)-2-((2-(6-chloro-1,2,3,4-tetrahydro-9H-carbazol-9-yl)-2-oxoethyl)amino)thiazol-4(5H)-one (10e). Yield; 130 mg (42 %); yellow solid; m.p.: 251–252 °C; IR (KBr, ύ cm^{-1}): 3350, 3219, 3036, 2935, 2856, 1701, 1686, 1604, 1558, 1456, 968, 733, 701, 635; ^{1}HNMR (400 MHz, DMSO-d_6) δ = 10.32 (brs, 1H; OH), 10.11 (t, *J*=5.7 Hz, 1H; NH), 8.20 (d, *J*=8.8 Hz, 1H; ArH-8 THC), 7.91 (s, 1H; =CH), 7.53 (d, *J*=2.2 Hz, 1H; ArH-5 THC), 7.38 (d, *J*=7.7 Hz, 1H; Ar'H), 7.30 (dd, *J*=8.8, 2.2 Hz, 1H; ArH-7 THC), 7.26 (dd, *J*=6.5, 1.7 Hz, 1H; Ar'H), 6.96 (t, *J*=7.6 Hz, 2H; Ar'H), 5.04 (d, *J*=4.5 Hz, 2H; CH_2NH), 3.03 (t, *J*=7.2 Hz, 2H; H-1 THC), 2.62 (t, *J*=6.9 Hz, 2H; H-4 THC), 1.94–1.71 (m, 4H; H-2, 3 THC); ^{13}CNMR (100 MHz, DMSO-d_6) δ = 179.6, 174.9, 168.1, 156.9, 136.3, 134.0, 131.4, *127.89*, *127.86*, 127.2, 125.1, 123.9, 121.0, 119.6, 117.6, 117.5, 117.3, 116.0, 49.3, 25.6, 23.2, 21.2, 20.6; Analysis calc.for $C_{24}H_{20}ClN_3O_3S$ (465.95):C, 61.86; H, 4.33; N, 9.02; S, 6.88. Found: C, 62.04; H, 4.60; N, 9.47; S, 7.01.

4.1.7.16. (Z)-5-(4-Hydroxybenzylidene)2-((2-(6-chloro-1,2,3,4-tetrahydro-9H-carbazol-9-yl)-2-oxoethyl)amino) thiazol-4(5H)-one (10f). Yield: 112 mg (36 %); yellow solid; m.p.: 203–206 °C; IR (KBr, ύ cm^{-1}): 3510, 3432, 3221, 3015, 2941, 2920, 2857, 1693, 1674, 1600, 1571, 1512, 1509, 1460, 954, 852, 720, 634; ^{1}HNMR (400 MHz, DMSO-d_6): 10.15 (brs, 1H; OH), 10.09 (t, *J*=5.6 Hz, 1H; NH), 8.19 (d, *J*=8.8 Hz, 1H; ArH-8 THC), 7.54 (s, 1H; =CH), 7.53 (d, *J*=2.0 Hz, 1H; ArH-5 THC), 7.44 (d, *J*=8.9 Hz, 2H; ArH-2′, 6′), 7.29 (dd, *J*=8.7, 2.0 Hz, 1H; ArH-7 THC), 6.92 (d, *J*=8.6 Hz, 2H; ArH-3′, 5′), 5.03 (d, *J*=4.7 Hz, 2H; CH_2NH), 3.03 (t, *J*=6.7 Hz, 2H; H-1 THC), 2.62 (t, *J*=6.9 Hz, 2H; H-4 THC), 1.91–1.75 (m, 4H; H-2, 3 THC); ^{13}CNMR (100 MHz, DMSO-d_6) δ = 179.7, 174.6, 168.2, 159.2, 136.3, 134.0, 131.7, 131.4, 130.5, 127.9, 124.8, 124.5, 123.9, 117.6, 117.5, 117.2, 116.2, 49.3, 25.6, 23.2, 21.2, 20.6; Analysis calc. for $C_{24}H_{20}ClN_3O_3S$ (465.95): C, 61.86; H, 4.33; N, 9.02; S, 6.88. Found: C, 61.70; H, 4.51; N, 9.23; S, 6.97.

4.1.7.17. (Z)-5-(4-Methoxybenzylidene)-2-((2-(6-chloro-1,2,3,4-tetrahydro-9H-carbazol-9-yl)-2-oxoethyl)amino)-thiazol-4(5H)-one (10g). Yield: 180 mg (56 %); yellow solid; m.p.: 253–255 °C; IR (KBr, ύ cm^{-1}): 3116, 3066, 2998, 2933, 2911, 2855, 2833, 1690, 1602, 1575, 1508, 1461, 968, 958, 822, 752, 633; ^{1}HNMR (400 MHz, DMSO-d_6) δ = 10.10 (brs, 1H; NH), 8.16 (d, *J*=8.2 Hz, 1H; ArH-8 THC), 7.55 (s, 1H; =CH), 7.53–7.47 (m, 3H; ArH-5 THC, ArH-2′, 6′), 7.26 (d, *J*=8.1 Hz, 1H; ArH-7 THC), 7.07 (d, *J*=8.6 Hz, 2H; ArH-3′, 5′), 5.01 (s, 2H; CH_2NH), 3.79 (s, 3H; CH_3O), 2.99 (brs, 2H; H-1 THC), 2.58 (brs, 2H; H-4 THC), 1.90–1.70 (m, 4H; H-2, 3 THC); ^{13}CNMR(100 MHz, DMSO-d_6) δ = 180.0, 175.1, 168.6, 160.9, 136.7, 134.5, 131.9, 130.4, 128.3, 126.8, 126.2, 124.3, 118.0, 117.9, 117.7, 115.3, 55.9, 49.8, 26.1, 23.6, 21.6, 21.0; Analysis calc. for $C_{25}H_{22}ClN_3O_3S$ (479.97): C, 62.56; H, 4.62; N, 8.75; S, 6.68. Found: C, 62.78; H, 4.75; N, 8.98; S,6.75.

4.1.7.18. (Z)-5-(3,4-Dimethoxybenzylidene)-2-((2-(6-chloro-1,2,3,4-tetrahydro-9H-carbazol-9-yl)-2-oxoethyl)amino)thiazol-4(5H)-one (10h). Yield: 155 mg (34 %); yellow solid; m.p.: 179–181 °C; IR (KBr, ύ cm^{-1}): 3362, 3132, 3087, 2995, 2962, 2916, 2867, 1675, 1610, 1597, 1568, 1547, 1510, 1462, 985, 969, 845, 794, 631; ^{1}H NMR (400 MHz, DMSO-d_6) δ = 10.11 (brs, 1H; NH), 8.19 (d, *J*=8.8 Hz, 1H; ArH-8 THC), 7.59 (s, 1H; =CH),7.53 (d, *J*=2.1 Hz, 1H; ArH-5 THC), 7.30 (dd, *J*=8.8, 2.2 Hz, 1H; ArH-7 THC), 7.20 (d, *J*=1.8 Hz, 1H; ArH-2′), 7.18 (dd, *J*=7.2, 1.8 Hz, 1H; ArH-6′), 7.13 (d, *J*=8.0 Hz, 1H; ArH-5′), 5.04 (s, 2H; CH_2NH), 3.83 (s, 6H; CH_3O), 3.03 (t, *J*=6.8 Hz, 2H; H-1 THC), 2.62 (t, *J*=6.9 Hz, 2H; H-4 THC), 1.91–1.75 (m, 4H; H-2, 3 THC); ^{13}C NMR (100 MHz, DMSO-d_6) δ = 180, 175.1, 168.5, 150.7, 149.4, 136.7, 134.5, 131.8, 130.8, 128.3, 127.1, 126.4, 124.3, 123.3, 118.0, 117.9, 117.7, 113.5, 112.6, 56.1, 56, 49.8, 40.9, 26.1, 23.6, 21.6, 21.0; Analysis calc. for $C_{26}H_{24}ClN_3O_4S$ (510.00): C, 61.23; H, 4.74; N, 8.24; S, 6.29. Found: C, 61.44; H, 4.85; N, 8.51; S, 6.37.

4.1.7.19. (Z)-5-(3,4,5-Trimethoxybenzylidene)-2-((2-(6-chloro-1,2,3,4-tetrahydro-9H-carbazol-9-yl)-2-oxoethyl)amino)thiazol-4(5H)-one (10i). Yield: 190 mg (53 %); yellow solid; m.p.: 203–205 °C; IR (KBr, ύ cm^{-1}): 3198, 2996, 2933, 2842, 1706, 1685, 1609, 1580, 1551, 1504, 1481, 966, 955, 896, 817, 755, 631; ^{1}HNMR (400 MHz, DMSO-d_6): 10.14 (brs, 1H; NH), 8.18 (d, *J*=8.9 Hz, 1H; ArH-8 THC),7.58 (s, 1H; =CH), 7.52 (d, *J*=2.3 Hz, 1H; ArH-5 THC), 7.29 (dd, *J*=8.8, 2.2 Hz, 1H; ArH-7 THC), 6.92 (s, 2H; ArH-2′, 6′), 5.04 (s, 2H; CH_2NH), 3.84 (s, 6H; CH_3O), 3.72 (s, 3H; CH_3O), 3.02 (t, *J*=7.6 Hz, 2H; H-1 THC), 2.61 (t, *J*=7.1 Hz, 2H; H-4 THC), 1.90–1.75 (m, 4H; H-2, 3 THC); ^{13}C NMR (100 MHz, DMSO-d_6) δ = 167.9, 153.4, 135.6, 134.7, 130.5, 130.1, 129.7, 124.4, 123.6, 118.5, 118.0, 115.8, 107.6, 60.5, 56.4, 49.5, 40.4, 25.8, 23.4, 21.4, 20.8; Analysis calc. for $C_{27}H_{26}ClN_3O_5S$ (540.03): C, 60.05; H, 4.85; N, 7.78; S, 5.94. Found: C, 60.23; H, 5.01; N, 8.05; S, 6.12.

4.1.7.20. (Z)-5-((E)-3-Phenylallylidene)-2-((2-(6-chloro-1,2,3,4-tetrahydro-9H-carbazol-9-yl)-2-oxoethyl)amino)thiazol-4(5H)-one (10j). Yield; 135 mg (44 %); yellow solid; m.p.: 256–258 °C; IR (KBr, ύ cm^{-1}): 3242, 2935, 2858, 1701, 1683, 1606, 1588, 1541, 1514, 1460, 967, 847, 744, 699; ^{1}HNMR (400 MHz, DMSO-d_6) δ = 10.11 (brs, 1H; NH), 8.19 (d, *J*=8.8 Hz, 1H; ArH-8 THC), 7.65 (d, *J*=7.4 Hz, 2H; ArH-2′, 6′), 7.53 (d, *J*=2.5 Hz, 1H; ArH-5 THC), 7.43–7.28 (m, 5H; ArH-7 THC, ArH-3′, 4′, 5′, =CH-CH=CH), 7.16 (d, *J*=15.3 Hz, 1H, =CH-CH=CH), 6.96 (dd, *J*=15.5, 11.3 Hz, 1H, =CH-CH=CH), 5.01 (s, 2H; CH_2NH), 3.02 (t, *J*=7.3 Hz, 2H; H-1 THC), 2.61 (t, *J*=6.9 Hz, 2H; H-4 THC), 1.91–1.74 (m, 4H; H-2, 3 THC); ^{13}C NMR (100 MHz, DMSO-d_6) δ = 178.9, 174, 168.2, 141.3, 136.3, 135.9, 134.0, 131.4, 131.1, 129.8, 129.3, 128.9, 127.9, 127.5, 125.2, 123.9, 117.6, 117.5, 117.3, 49.2, 25.6, 23.2, 21.2, 20.6; Analysis calc for $C_{26}H_{22}ClN_3O_2S$ (475.99): C, 65.61; H, 4.66; N, 8.83; S, 6.74. Found: C, 65.42; H, 4.78; N, 9.07; S, 6.85.

4.2. Biological evaluation

4.2.1. Cytotoxic activity using SRB assay and evaluation of IC_{50}

The following cell lines were kept at the Molecular Pharmacology lab: MCF7, MDA-MB-231 (breast cancer), colon HCT-116, lung A549, Jurkart leukemia, and U937 Histiocytic lymphoma. Cells were kept at 37 °C in a humidified environment with 5 % CO_2 and were supplemented with 10 % heat inactivated FBS, 50 units/mL of penicillin, and 50 g/mL of streptomycin (all from Sigma). By repeatedly subculturing the cells, the "monolayer culture" was preserved. Cytotoxicity was assessed by means of the SRB technique. Using 0.25 % trypsin-EDTA, exponentially developing cells were harvested and planted at a density of 1000–2000 cells/well in supplemented DMEM media in 96-well plates. Cells were treated with varying concentrations of the tested compound(s), reference drug (doxorubicin), or vehicle (DMSO) for 48 h. The cells were fixed with 50 % trichloroacetic acid for 1 h at 4 °C. Wells were stained with 0.4 % SRB dissolved in 1 % acetic acid for 10 min at room temperature. After allowing the plates to air dry for a full day, the dye was dissolved using Tris HCl for five minutes at 1600 rpm on a shaker. Using nonlinear regression models and the Boltzmann sigmoidal concentration response curve equation, the IC_{50} values were determined (GraphPad, Prism Version 5). The stated outcomes are the averages of a minimum of three independent studies. One-way ANOVA was used to examine significant differences, and $P<0.05$ indicated that the differences were significant. The maximum concentration of DMSO employed to dissolve the compounds was utilized to culture control (untreated) cells. DMSO concentrations in all samples were less than or equal to 0.1 %.

4.2.2. Effect on normal lymphocytes

The pure culture of normal human lymphocytes (PCS-800–017) was obtained from VACSERA. Remove cultures from incubator into laminar flow hood or other sterile work area. Then reconstitute each vial of the tested compounds **9d**, **10e**, **10f**, and **10g** [15 mg/vial in serum vial] to be used with 3 ml of medium or balanced salt solution without phenol red and serum. Followed by the Addition of the reconstituted MTT (3-[4,5-dimethylthiazol-2-yl]-2,5-diphenyl tetrazolium bromide) in an amount equal to 10 % of the culture medium volume. Return cultures to incubator for 2–4 h. After the incubation period, remove cultures from incubator and dissolve the resulting formazan crystals by adding an amount of MTT Solubilization Solution 10 % Triton X-100 plus 0.1 N HCl in anhydrous isopropanol, 125 ml, which equal to the original culture medium volume. Gentle mixing in a gyratory shaker will enhance dissolution. Spectrophotometrically measure absorbance at a wavelength of 570 nm, by measuring the background absorbance of multiwell plates at 690 nm and subtract from the 570 nm measurement [73].

4.2.3. Cell cycle analysis

The cell cycle analysis protocol was applied based on the quantitation of the amount of DNA stained by propidium iodide. After treatment of the Jurkat cell lines with the tested compound (**10e**) for the specified duration, cells (105 cells) are collected by trypsinization and washed twice with ice-cold PBS (pH 7.4). Cells are resuspended in two milliliters of 60 % ice-cold ethanol and incubated at 4 °C for 1 h for fixation. Fixed cells are washed twice again with PBS (pH 7.4) and re-suspended in 1 mL of PBS containing 50 μg/mL RNAase A and 10 μg/mL propidium iodide (PI). After 20 min of incubation in dark at 37 °C, Jurkat cells are analyzed for DNA contents using flow cytometric analysis using FL2 (λex/em 535/617 nm) signal detector (ACEA Novocyte™ flow cytometer, ACEA Biosciences Inc., San Diego, CA, USA) [74].

4.2.4. Cell apoptosis assay

The assay depends on the translocation of phosphatidylserine (PS) after apoptosis initiation to the cell surface. Where PS can be stained using the high affinity protein fluorescent conjugate of annexin V. The

effect of tested compound **10e** on apoptosis induction was investigated using annexin V-FITC/PI apoptosis detection kit (Biovision, K101-25). Propidium iodide (PI) was used as a counterstain and Annexin V fluorescein isothiocyanate (FITC) staining agent for Jurkat cells in this experiment. Then, Jurkat cells in densities of 2×10^5 per well were incubated with compounds **10e** for 48 h. After trypsinization, the cells were stained for 15 min at 37 °C in the dark and then rinsed with phosphate-buffered saline (PBS) [75].

4.2.5. VEGFR-2 enzyme assay

Using a VEGFR-2 kinase assay kit (Bioscience), the most active compounds were evaluated against the VEGFR-2 enzyme. Its goal is to quantify VEGFR2 activity in order to screen using Kinase-Glo® MAX as the detection reagent. The IC_{50} of each of the four drugs was determined by comparing them to the control and utilizing the concentration-inhibition response curve in relation to the in comparison with the reference medicine, sorafenib. 6 µl of 5x Kinase assay buffer, 1 µl ATP (500 µM), 1 µl 50x PTK substrate, and 17 µl of water were used to form the master mixture (25 µl per well). Add 5 µl of each well-labeled "Test Inhibitor" solution of **9d**, **10e**, **10f** and **10g**. The same solution (inhibitor buffer) was added in 5 µl for the "Positive Control" and "Blank". 3 ml of 1x Kinase assay buffer were prepared by mixing 600 µl of 5x Kinase assay buffer with 2400 µl water. To the wells designated as "Blank", add 20 µl of 1x Kinase assay buffer. The VEGFR-2 enzyme was thawed on ice. Upon first thaw, briefly spin tube containing enzyme to recover full content of the tube. The test requires a determined amount of VEGFR-2, which should be diluted with 1x Kinase assay buffer to a concentration of 1 ng/µl. Next, start the reaction by filling the "Positive Control" and "Test Inhibitor Control" wells with 20 µl of diluted VEGFR-2 enzyme. For 40 min, incubate at 30 °C. Thaw the Kinase-Glo Max reagent after that. Once the reaction has been going for 40 min, put 50 µl of Kinase-Glo Max reagent in each well. After covering the plate with aluminum foil and letting it sit at room temperature for 15 min, use a microplate reader to measure the luminescence. Lastly, using the dose response curve and sorafenib as a reference medication, the IC_{50} of the investigated compounds was determined [76].

4.2.6. EGFR enzyme assay

Compounds were tested against EGFR enzyme using EGFR kinase assay kit (Bioscience). It is designed to measure EGFR activity for the purpose of screening via Kinase-Glo® MAX as detection reagent. The four compounds (**9d**, **10e**, **10f**, and **10g**) were compared to control and the IC_{50} of each compound were calculated using the concentration-inhibition response curve compared to reference drug erlotinib. The master mixture (25 µl per well) was prepared using 6 µl 5x Kinase assay buffer + 1 µl ATP (500 µM) + 1 µl 50x PTK substrate + 17 µl water. Add 5 µl of Inhibitor solution **9d**, **10e**, **10f**, and **10g** of each well labeled as "Test Inhibitor". For the "Positive Control" and "Blank", 5 µl were added of the same solution without inhibitor (Inhibitor buffer). 3 ml of 1x Kinase assay buffer were prepared by mixing 600 µl of 5x Kinase assay buffer with 2400 µl water. To the wells designated as "Blank", add 20 µl of 1x Kinase assay buffer. The EGFR enzyme was thawed on ice. Upon first thaw, briefly spin tube containing enzyme to recover full content of the tube. The amount of EGFR calculated required for the assay and dilute enzyme to 1 ng/µl with 1x Kinase assay buffer. Then initiate reaction by adding 20 µl of diluted EGFR enzyme to the wells designated "Positive Control" and "Test Inhibitor Control". Incubate at 30 °C for 40 min. After that, thaw Kinase-Glo Max reagent. After the 40-min reaction, add 50 µl of Kinase-Glo Max reagent to each well. Cover the plate with aluminum foil and incubate the plate at room temperature for 15 min then measure luminescence using the microplate reader. Finally, The IC_{50} of tested compounds were measured using the dose response curve against erlotinib as a reference drug [77].

4.2.7. Tubulin enzyme assay

Tubulin Polymerization assay was performed using a highly purified tubulin from porcine brain. The commercial kit was acquired from Cytoskeleton (Danvers, MA, USA), with the product code BK011P. First, Plate cells (1.2–1.8 × 10,000 cells/well) in a 96-well plate containing 100 µL solution of the tested compounds **9d**, **10e**, and **10g** per well and 100 µL of full growth media for 18–24 h. After incubation, solutions were withdrawn, and trypsinization was used to separate the cells. The cells were then suspended in PBS, rinsed with cold PBS buffer, and subjected to three freeze/thaw cycles to lyse them. To identify β-tubulin in the supernatant, cell lysates were spun for 10 min in a cooled centrifuge to eliminate cellular debris. Following that, standards or cell lysate samples were added to the corresponding microtiter plate wells that had been coated with an antibody specific to TUBb that conjugated with biotin. Only after adding the TMB substrate solution. Each micro plate well is then filled with horseradish peroxidase (HRP)-conjugated avidin and incubated. Only the wells containing TUBb, biotin-conjugated antibody, and enzyme-conjugated avidin will show a characteristic color change upon the addition of TMB substrate solution. Sulfuric acid solution is added to stop the enzyme substrate reaction, and the color change is quantified spectrophotometrically in triplicate using an ELISA reader (Tecan Spark reader) at 450 ± 10 nm. The decrease of color intensity was measured as a sign of tubulin inhibition. The OD of the samples was then compared to the standard curve to determine the concentration of TUBb at 10 µM in the samples. [78].

4.3. Molecular docking studies

All the molecular modeling calculations and docking simulation studies were performed on a Processor Intel(R) Pentium(R) CPU N3510@ 1.99 GHz and 4 GB Memory with Microsoft Windows 8.1 pro (64 Bit) operating system using Molecular Operating Environment (MOE 2019.0102, 2020; Chemical Computing Group, Canada) as the computational software. All MOE minimizations were performed until a RMSD gradient of 0.01 kcal/mol/Å with the force field (Amber10:EHT) to calculate the partial charges automatically using R Field solvation. In case of EGFR, all minimizations were performed using the force field (OPLS-AA) as well as Born solvation model. Before simulations, the protein was corrected, hydrogens are added and ionization states assigned, water layer was modeled and the system was optimized via protonation, and receptor was minimized using QuickPrep function. Then, both ligand and pocket were isolated in 3D and molecular surface was drawn around the binding site to visualize the space available for docked ligands. The compounds' database was created after the compounds' structures were prepared, partially charged, and minimized. Initially, Self-docking was performed, and ligand conformations are generated with the bond rotation method. These are then placed on the site with the Triangle Matcher method and ranked with the London dG scoring function. The Retain option specifies the number of poses (30) to pass to the Refinement, for energy minimization in the pocket, before restoring with the GBVI/WSA dG scoring function. Docking simulation was performed using compound database mdb file. A triangle matching with London dG scoring was chosen for initial placement, and then the top 30 poses were refined using force field (Amber10:EHT for VEGFR-2 or tubulin, OPLS-AA for EGFR) and GBVI/WSA dG scoring. The output database dock file was created with different poses for each ligand and arranged according to the final score function (S), which is the score of the last stage that was not set to zero.

CRediT authorship contribution statement

Basma S. Ali: Writing – review & editing, Methodology, Investigation, Visualization, Validation, Data curation, Formal analysis. **Anber F. Mohammed:** Writing – review & editing, Visualization, Validation, Supervision, Software, Resources, Formal analysis, Data curation. **Benson M. Kariuki:** Writing – review & editing, Visualization, Validation, Formal analysis, Data curation. **Raafat El-Awady:** Writing – review & editing, Visualization, Validation, Supervision, Software, Methodology,

Investigation, Formal analysis, Data curation. **Hajjaj H. M. Abdu-Allah:** Writing – review & editing, Validation, Supervision, Software, Resources, Project administration, Methodology, Investigation, Funding acquisition, Conceptualization.

Declaration of competing interest

The authors declare that they have no known competing financial interests or personal relationships that could have appeared to influence the work reported in this paper.

Appendix A. Supplementary data

Supplementary data to this article can be found online at https://doi.org/10.1016/j.bioorg.2024.107817.

References

[1] F. Bray, M. Laversanne, H. Sung, J. Ferlay, R.L. Siegel, I. Soerjomataram, A. Jemal, Global cancer statistics 2022: GLOBOCAN estimates of incidence and mortality worldwide for 36 cancers in 185 countries, CA Cancer J Clin. 74 (2024) 229-263.

[2] A. Sochacka-Ćwikła, M. Mączyński, A. Regiec, FDA-approved drugs for hematological malignancies—the last decade review, Cancers. 14 (2021) 87.

[3] T. Meenaghan, M. Dowling, M. Kelly, Acute leukaemia: making sense of a complex blood cancer, Br. J. Nurs. 21 (2012) 76–83.

[4] T. Dai, L. Lin, H. Chen, W. Lu, X. Yang, L. Yang, Y. Liu, J. Cui, D. Sun, Novel nitrogen mustard-artemisinin hybrids with potent anti-leukemia action through DNA damage and activation of GPx, Eur. J. Med. Chem. 244 (2022) 114783.

[5] A. Doostmohammadi, H. Jooya, K. Ghorbanian, S. Gohari, M. Dadashpour, Signaling, Potentials and future perspectives of multi-target drugs in cancer treatment: the next generation anti-cancer agents, Cell. Commun. Signal. 22 (2024) 228.

[6] M.K. Paul, A.K. Mukhopadhyay, Tyrosine kinase - Role and significance in Cancer, Int. J. Med. Sci. 1 (2004) 101–115.

[7] W.M. Eldehna, G.H. Al-Ansary, T. Al-Warhi, M.Y. Jaballah, M. Elaasser, M. Rashed, Identification of novel ureido benzothiophenes as dual VEGFR-2/EGFR anticancer agents, Bioorg. Chem. 143 (2024) 107037.

[8] Y. Liu, Y. Li, Y. Wang, C. Lin, D. Zhang, J. Chen, L. Ouyang, F. Wu, J. Zhang, L. Chen, Oncology, Recent progress on vascular endothelial growth factor receptor inhibitors with dual targeting capabilities for tumor therapy, Hematol. Oncol. 15 (2022) 89.

[9] M.R. Raspollini, F. Castiglione, F. Garbini, A. Villanucci, G. Amunni, G. Baroni, V. Boddi, G.L. Taddei, Correlation of Epidermal Growth Factor Receptor Expression with Tumor Microdensity Vessels and with Vascular Endothelial Growth Factor Expression in Ovarian Carcinoma, Int. J. Surg. Pathol. 13 (2005) 135–142.

[10] S. Di Martino, A. Rainone, A. Troise, M. Di Paolo, S. Pugliese, S. Zappavigna, A. Grimaldi, D. Valente, Overview of FDA-approved anti cancer drugs used for targeted therapy, WCRJ. 2 (2015) e553.

[11] M. Shibuya, Vascular Endothelial Growth Factor (VEGF) and Its Receptor (VEGFR) Signaling in Angiogenesis: A Crucial Target for Anti- and Pro-Angiogenic Therapies, Genes, Cancer. 2 (2011) 1097–1105.

[12] X.-J. Liu, H.-C. Zhao, S.-J. Hou, H.-J. Zhang, L. Cheng, S. Yuan, L.-R. Zhang, J. Song, S.-Y. Zhang, S.-W. Chen, Recent development of multi-target VEGFR-2 inhibitors for the cancer therapy, Bioorg. Chem. 133 (2023) 106425.

[13] T. Al-Warhi, A.M. El Kerdawy, M.A. Said, A. Albohy, Z.M. Elsayed, N. Aljaeed, E. B. Elkaeed, W.M. Eldehna, H.A. Abdel-Aziz, M.A. Abdelmoaz, Novel 2-(5-Aryl-4,5-Dihydropyrazol-1-yl)thiazol-4-One as EGFR Inhibitors: Synthesis, Biological Assessment and Molecular Docking Insights, Drug. Des. Devel. Ther. 16 (2023) 1457–1471.

[14] J.Z. Sun, Y. Lu, Y. Xu, F. Liu, F.Q. Li, Q.L. Wang, C.T. Wu, X.W. Hu, H.F. Duan, Epidermal growth factor receptor expression in acute myelogenous leukaemia is associated with clinical prognosis, Hematol. Oncol. 30 (2012) 89–97.

[15] L. Saryeddine, K. Zibara, N. Kassem, B. Badran, N. El-Zein, EGF-induced VEGF exerts a PI3K-dependent positive feedback on ERK and AKT through VEGFR2 in hematological in vitro models, PLoS One. 11 (2016) e0165876.

[16] T.R. Jackson, A. Vuorinen, L. Josa-Culleré, K.S. Madden, D. Conole, T.J. Cogswell, I.V. Wilkinson, L.M. Kettyle, D. Zhang, A. O'Mahony, A tubulin binding molecule drives differentiation of acute myeloid leukemia cells, iScience. 25 (2022) 104787.

[17] M. Barreca, A. Stathis, P. Barraja, F. Bertoni, An overview on anti-tubulin agents for the treatment of lymphoma patients, Pharmacol. Ther. 211 (2020) 107552.

[18] J. Zhang, X. Liu, N. Sa, J.H. Zhang, Y.S. Cai, K.M. Wang, W. Xu, C.S. Jiang, K. K. Zhu, Synthesis and biological evaluation of 1-phenyl-tetrahydro-β-carboline-based first dual PRMT5/EGFR inhibitors as potential anticancer agents, Eur. J. Med. Chem. 269 (2024) 116341.

[19] N. Kumar, P. Gupta, Anticancer Tetrahydrocarbazoles: A Wide Journey from 2000 Till Date, Lett. Drug. Des. Discov.21 (2022) 421-439.

[20] R.A. Bohannon, D.G. Miller, H.D. Diamond, Vincristine in the treatment of lymphomas and leukemias, Cancer. Res. 23 (1963) 613–621.

[21] G.-H. Du, Vinblastine and vincristine, in:Y.-W. Zhang, X.-Y. Kong, J.-H. Wang, G.-H. Du (First ed.), Natural Small Molecule Drugs from Plants, Springer, Berlin/Heidelberg, Germany, 2018, pp. 551-557.

[22] E.S. Kim, Midostaurin: first global approval, Drugs. 77 (2017) 1251–1259.

[23] L. Cao, M. Weetall, C. Trotta, K. Cintron, J. Ma, M.J. Kim, B. Furia, C. Romfo, J. D. Graci, W. Li, J. Du, J. Sheedy, J. Hedrick, N. Risher, S. Yeh, H. Qi, T. Arasu, S. Hwang, W. Lennox, R. Kong, J. Petruska, Y.C. Moon, J. Babiak, T.W. Davis, A. Jacobson, N.G. Almstead, A. Branstrom, J.M. Colacino, S.W. Peltz, Targeting of hematologic malignancies with PTC299, a novel potent inhibitor of dihydroorotate dehydrogenase with favorable pharmaceutical properties, Mol. Cancer. Ther. 18 (2019) 3–16.

[24] T. Indumathi, A. Muthusankar, P. Shanmughavel, K.R.J. Prasad, Synthesis of heteroannulated carbazoles: exploration of *in vitro* cytotoxicity and molecular docking studies, Med. Chem. Commun. 4 (2013) 450–455.

[25] A.A. Failli, R.J. Steffan, A.F. Kreft, T.J. Caggiano, C.E. Caufield, Pyranoindole and tetrahydrocarbazole inhibitors of COX-2, US1998/5830911A.

[26] T. Schuster, K. Paulini, P. Schmidt, S. Baasner, E. Polymeropoulos, E. Guenther, M. Teifel, Tetrahydrocarbazole derivatives as ligands of G-protein coupled receptors, US2012/8148546B2.

[27] W. Deng, D. Chen, Bicyclic heterocycles hydroxamate compounds useful as histone deacetylase (HDAC) inhibitors, WO2006/101456.

[28] M.P. Bernard, S. Bancos, P.J. Sime, R.P. Phipps, Targeting cyclooxygenase-2 in hematological malignancies: rationale and promise, Curr. Pharm. Des. 14 (2008) 2051–2060.

[29] P. Roszczenko, S. Holota, O.K. Szewczyk, R. Dudchak, K. Bielawski, A. Bielawska, R. Lesyk, 4-Thiazolidinone-bearing hybrid molecules in anticancer drug design, Int. J. Mol. Sci. 23 (2022) 13135.

[30] I. Subtelna, A. Kryshchyshyn-Dylevych, R. Jia, M. Lelyukh, A. Ringler, S. Kubicek, O. Zagrijtschuk, R. Kralovics, R. Lesyk, 5-Arylidene-2-(4-hydroxyphenyl) aminothiazol-4(5H)-ones with selective inhibitory activity against some leukemia cell lines, Arch. Pharm. 354 (2021) e2000342.

[31] K.-M. Qiu, H.-H. Wang, L.-M. Wang, Y. Luo, X.-H. Yang, X.-M. Wang, H.-L. Zhu, Design, synthesis and biological evaluation of pyrazolyl-thiazolinone derivatives as potential EGFR and HER-2 kinase inhibitors, Bioorg. Med. Chem. 20 (2012) 2010–2018.

[32] M.M. El-Miligy, H.A.A.E. Razik, M.M. Abu-Serie, Synthesis of piperazine-based thiazolidinones as VEGFR2 tyrosine kinase inhibitors inducing apoptosis, Future, Med. Chem. 9 (2017) 1709–1729.

[33] k. Venu, B. Saritha, B.B.V. Sailaja, New molecular hybrids containing benzimidazole, thiazolidine-2,4-dione and 1,2,4-oxadiazole as EGFR directing cytotoxic agents, Tetrahedron. 124 (2022) 132991.

[34] N. Shalmali, S. Bawa, M.R. Ali, S. Kalra, R. Kumar, B. Zeya, M.A. Rizvi, S. Partap, A. Husain, Molecular docking and in vitro anticancer screening of synthesized arylthiazole linked 2H-indol-2-one derivatives as VEGFR-2 kinase inhibitors, Anticancer. Agents, Med. Chem. 22 (2022) 2166–2180.

[35] D.K. Sigalapalli, V. Pooladanda, P. Singh, M. Kadagathur, S.D. Guggilapu, J. L. Uppu, N.D. Tangellamudi, P.K. Gangireddy, C. Godugu, N.B. Bathini, Discovery of certain benzyl/phenethyl thiazolidinone-indole hybrids as potential anti-proliferative agents: Synthesis, molecular modeling and tubulin polymerization inhibition study, Bioorg. Chem. 92 (2019) 103188.

[36] A. Kryshchyshyn-Dylevych, L. Radko, N. Finiuk, M. Garazd, N. Kashchak, A. Posyniak, K. Niemczuk, R. Stoika, R. Lesyk, Synthesis of novel indole-thiazolidinone hybrid structures as promising scaffold with anticancer potential, Bioorg. Med. Chem 50 (2021) 116453.

[37] A. Sharma, D. Sharma, N. Saini, S.V. Sharma, V.K. Thakur, R.K. Goyal, P. C. Sharma, Recent advances in synthetic strategies and SAR of thiazolidin-4-one containing molecules in cancer therapeutics, Cancer. Metastasis. Rev. 42 (2023) 847–889.

[38] C. Bathula, S. Tripathi, R. Srinivasan, K.K. Jha, A. Ganguli, G. Chakrabarti, S. Singh, P. Munshi, S. Sen, Synthesis of novel 5-arylidenethiazolidinones with apoptotic properties via a three-component reaction using piperidine as a bifunctional reagent, Org. Biomol. Chem. 14 (2016) 8053–8063.

[39] W.S. Ramadan, M.M. Saber-Ayad, E. Saleh, H.H.M. Abdu-Allah, A. Abdel-nasser, V. Menon, H. Tarazi, M.H. Semreen, N.C. Soares, S. Hafezi, Design, synthesis and mechanistic anticancer activity of new acetylated 5-aminosalicylate-thiazolinone hybrid derivatives, iScience. 27 (2024) 108659.

[40] W.S. Ramadan, E.M. Saleh, V. Menon, C.G. Vazhappilly, H.H.M. Abdu-Allah, A.-N.-A. El-Shorbagi, W. Mansour, R. El-Awady, Pharmacotherapy, Induction of DNA damage, apoptosis and cell cycle perturbation mediate cytotoxic activity of new 5-aminosalicylate–4-thiazolinone hybrid derivatives, Biomed. Pharmacother. 131 (2020) 110571.

[41] S.A. Othman, O.F. Abou-Ghadir, W.S. Ramadan, Y.A. Mostafa, R. El-Awady, H.H. M. Abdu-Allah, The design, synthesis, biological evaluation, and molecular docking of new 5-aminosalicylamide-4-thiazolinone hybrids as anticancer agents, Arch. Pharm. 356 (2023) 2300315.

[42] C.G. Vazhappilly, E. Saleh, W. Ramadan, V. Menon, A.M. Al-Azawi, H. Tarazi, H.H. M. Abdu-Allah, A.-N. El-Shorbagi, R. El-Awady, Inhibition of SHP2 by new compounds induces differential effects on RAS/RAF/ERK and PI3K/AKT pathways in different cancer cell types, Invest. New, Drugs. 37 (2019) 252–261.

[43] H.H.M. Abdu-Allah, S.G. Abdel-Moty, R. El-Awady, A.-N.-A. El-Shorbagi, Design and synthesis of novel 5-aminosalicylate (5-ASA)–4-thiazolinone hybrid derivatives with promising antiproliferative activity, Bioorg. Med. Chem. Lett. 26 (2016) 1647–1650.

[44] M. Saravanabhavan, A.F. Ebenazer, V. Murugesan, M. Sekar, Synthesis, Spectroscopic Characterization and Biological Evaluation of 1-(4'-Hydroxybenzamido)-Imine-1, 2, 3, 4-Tetrahydrocarbazole Derivatives, J. Adv. Phys. 6 (2017) 30–40.

[45] L. Cao, M. Weetall, J. Bombard, H. Qi, T. Arasu, W. Lennox, J. Hedrick, J. Sheedy, N. Risher, P.C. Brooks, Discovery of novel small molecule inhibitors of VEGF

expression in tumor cells using a cell-based high throughput screening platform, PLoS One. 11 (2016) e0168366.
[46] P. Chikkegowda, B.C. Pookunoth, V.R. Bovilla, P.M. Veeresh, Z. Leihang, T. Thippeswamy, M.A. Padukudru, B. Hathur, R.S. Kanchugarakoppal, Basappa, Design, synthesis, characterization, and crystal structure studies of Nrf2 modulators for inhibiting cancer cell growth in vitro and in vivo, ACS, Omega. 6 (2021) 10054–10071.
[47] N.H. Metwally, M.A. Abdalla, M.A.N. Mosselhi, E.A. El-Desoky, Synthesis and antimicrobial activity of some new N-glycosides of 2-thioxo-4-thiazolidinone derivatives, Carbohydr. Res. 345 (2010) 1135–1141.
[48] K. Bourahla, S. Guihéneuf, E. Limanton, L. Paquin, R. Le Guével, T. Charlier, M. Rahmouni, E. Durieu, O. Lozach, F. Carreaux, Design and microwave Synthesis of New (5 Z) 5-Arylidene-2-thioxo-1, 3-thiazolinidin-4-one and (5 Z) 2-Amino-5-arylidene-1, 3-thiazol-4 (5 H)-one as New Inhibitors of Protein Kinase DYRK1A, Pharmaceuticals. 14 (2021) 1086.
[49] S. Kambe, V. Thiocyanoacetate, Reaction of Thiocyanoacetic Esters with Aromatic Aldehydes in the Presence of Potassium Acetate, Bull. Chem. Soc. Jpn. 46 (1973) 2926–2928.
[50] B.A. Dalvi, P.D. Lokhande, Copper(II) catalyzed aromatization of tetrahydrocarbazole: An unprecedented protocol and its utility towards the synthesis of carbazole alkaloids, Tetrahedron. Lett. 59 (2018) 2145–2149.
[51] A. Sandvoß, J.M. Wahl, From Cycloalkanols to Heterocycles via Nitrogen Insertion, Org Lett. 25 (2023) 5795–5799.
[52] A. Sudhakara, H. Jayadevappa, H.N.H. Kumar, K.M. Mahadevan, Bismuth Nitrate Promoted Fischer Indole Synthesis: A Simple and Convenient Approach for the Synthesis of Alkyl Indoles, Lett. Org. Chem. 6 (2009) 159–164.
[53] M. Zhang, F. Xie, X. Wang, F. Yan, T. Wang, M. Chen, Y. Ding, Improved indole syntheses from anilines and vicinal diols by cooperative catalysis of ruthenium complex and acid, RSC, Advances 3 (2013) 6022–6029.
[54] L. KEXIN, T. GUOTAO, X. RUNDE, D. XIANGPING, Indolamide compound with anti-tumor activity, CN2018/108912035A.
[55] J.J. Li, Delépine amine synthesis, in: J.J. Li, Name reactions: a collection of detailed mechanisms and synthetic applications (Fourth ed), Springer, Verlag Berlin Heidelberg, 2009, pp. 171-172.
[56] M. Sarkis, D.N. Tran, S. Kolb, M.A. Miteva, B.O. Villoutreix, C. Garbay, E. Braud, Design and synthesis of novel bis-thiazolone derivatives as micromolar CDC25 phosphatase inhibitors: Effect of dimerisation on phosphatase inhibition, Bioorg. Med. Chem. Lett. 22 (2012) 7345–7350.
[57] I. Subtel'na, D. Atamanyuk, E. Szymańska, K. Kieć-Kononowicz, B. Zimenkovsky, O. Vasylenko, A. Gzella, R. Lesyk, Synthesis of 5-arylidene-2-amino-4-azolones and evaluation of their anticancer activity, Bioorg. Med. Chem. 18 (2010) 5090-5102.
[58] Y.M. Omar, H.H.M. Abdu-Allah, S.G. Abdel-Moty, Synthesis, biological evaluation and docking study of 1,3,4-thiadiazole-thiazolidinone hybrids as anti-inflammatory agents with dual inhibition of COX-2 and 15-LOX, Bioorg. Chem. 80 (2018) 461–471.
[59] T. Padró, R. Bieker, S. Ruiz, M. Steins, S. Retzlaff, H. Bürger, T. Büchner, T. Kessler, F. Herrera, J. Kienast, C. Müller-Tidow, H. Serve, W.E. Berdel, R.M. Mesters, Overexpression of vascular endothelial growth factor (VEGF) and its cellular receptor KDR (VEGFR-2) in the bone marrow of patients with acute myeloid leukemia, Leukemia. 16 (2002) 1302–1310.
[60] S.J. Modi, V.M. Kulkarni, Vascular endothelial growth factor receptor (VEGFR-2)/KDR inhibitors: medicinal chemistry perspective, Med. Drug. Discov. 2 (2019) 100009.
[61] J.K. Buolamwini, Cell cycle molecular targets in novel anticancer drug discovery, Curr. Pharm. Des. 6 (2000) 379–392.
[62] V. Grunwald, M. Hidalgo, Developing inhibitors of the epidermal growth factor receptor for cancer treatment, J. Natl. Cancer. Inst. 95 (2003) 851–867.
[63] Chemical Computing Group ULC, Molecular Operating Environment (MOE), 2019.01, Chemical Computing Group ULC, Montreal, Canada .2020.
[64] M. McTigue, B.W. Murray, J.H. Chen, Y.-L. Deng, J. Solowiej, R.S. Kania, Molecular conformations, interactions, and properties associated with drug efficiency and clinical performance among VEGFR TK inhibitors, Proc. Natl. Acad. Sci U S a. 109 (2012) 18281–18289.
[65] J. Stamos, M.X. Sliwkowski, C. Eigenbrot, Structure of the epidermal growth factor receptor kinase domain alone and in complex with a 4-anilinoquinazoline inhibitor, J. Biol. Chem. 277 (2002) 46265–46272.
[66] A.B. Waight, K. Bargsten, S. Doronina, M.O. Steinmetz, D. Sussman, A.E. Prota, Structural basis of microtubule destabilization by potent auristatin anti-mitotics, PLoS One. 11 (2016) e0160890.
[67] J. Wang, D.D. Miller, W. Li, Molecular interactions at the colchicine binding site in tubulin: An X-ray crystallography perspective, Drug. Discov. Today. 27 (2022) 759–776.
[68] S.A. Patil, R. Patil, D.D. Miller, Indole molecules as inhibitors of tubulin polymerization: potential new anticancer agents, Future, Med. Chem. 4 (2012) 2085–2115.
[69] R. Gaspari, A.E. Prota, K. Bargsten, A. Cavalli, M.O. Steinmetz, Structural basis of cis-and trans-combretastatin binding to tubulin, Chem. 2 (2017) 102–113.
[70] C. Boureghda, R. Boulcina, V. Dorcet, F. Berrée, B. Carboni, A. Debache, Facile synthesis of 5-arylidene rhodanine derivatives using Na_2SO_3 as an eco-friendly catalyst. Access to 2-mercapto-3-aryl-acrylic acids and a benzoxaborole derivative, Tetrahedron. Lett. 62 (2021) 152690.
[71] K.M. Noorulla, A.J. Suresh, V. Devaraji, B. Mathew, D. Umesh, Molecular modeling of drug-pathophysiological Mtb protein targets: Synthesis of some 2-thioxo-1, 3-thiazolidin-4-one derivatives as anti-tubercular agents, J. Mol. Struct. 1147 (2017) 682–696.
[72] K. Gong, Z.-W. He, Y. Xu, D. Fang, Z. Liu, Green synthesis of 5-benzylidene rhodanine derivatives catalyzed by 1-butyl-3-methyl imidazolium hydroxide in water, Monatsh. Chem. 139 (2008) 913–915.
[73] M.M. Zeid, O.M. El-Badry, S. Elmeligie, R.A. Hassan, Design, synthesis, and molecular docking of novel miscellaneous chalcones as p38α mitogen-activated protein kinase inhibitors, Chem Biodivers. 21 (2024) e202400077.
[74] J. Wang, M.J. Lenardo, Roles of caspases in apoptosis, development, and cytokine maturation revealed by homozygous gene deficiencies, J. Cell. Sci. 113 (2000) 753–757.
[75] I.H. Eissa, M.A. Dahab, M.K. Ibrahim, N.A. Alsaif, A.Z. Alanazi, S.I. Eissa, A.B. M. Mehany, A.M. Beauchemin, Design and discovery of new antiproliferative 1,2,4-triazin-3(2H)-ones as tubulin polymerization inhibitors targeting colchicine binding site, Bioorg. Chem. 112 (2021) 104965.
[76] A.E. Kassab, Y. El-Dash, E.M. Gedawy, Novel pyrazolopyrimidine urea derivatives: Synthesis, antiproliferative activity, VEGFR-2 inhibition, and effects on the cell cycle profile, Arch. Pharm. 353 (2020) 1900319.
[77] R.Z. Batran, S.M. El-Daly, W.A. El-Kashak, E.Y. Ahmed, Design, Design, synthesis, and molecular modeling of quinoline-based derivatives as anti-breast cancer agents targeting EGFR/AKT signaling pathway, Chem. Biol. Drug. Des. 99 (2022) 470–482.
[78] M. Mustafa, S. Anwar, F. Elgamal, E.R. Ahmed, O.M. Aly, Potent combretastatin A-4 analogs containing 1,2,4-triazole: Synthesis, antiproliferative, anti-tubulin activity, and docking study, Eur. J. Med. Chem. 183 (2019) 111697.